A NON-PARAMETRIC ALGORITHM FOR TIME-DEPENDENT MODAL ANALYSIS OF CIVIL STRUCTURES AND INFRASTRUCTURES

Manuel F. Hormazábal[1]; Alberto Barontini[1]; Maria Giovanna Masciotta[2]; Daniel V. Oliveira[1]

[1] ISISE, Department of Civil Engineering, University of Minho, Campus de Azurém, 4800-058 Guimarães, Portugal.
[2] Department of Engineering and Geology (InGeo), G. d'Annunzio University of Chieti–Pescara, Viale Pindaro 42, 65127, Pescara, Italy.

Emails: m.hormazabal@gmail.com, albe.barontini@gmail.com, g.masciotta@unich.it, danvco@civil.uminho.pt

Abstract

Vibration-based monitoring strategies have been demonstrated to be effective tools in providing – in nearly real-time – reliable information regarding the integrity of structures and infrastructure systems. However, commonly used methods for vibration analysis and modal identification are not able to capture the time variation of the modal properties during single acquisitions, hence they cannot perform dynamic identification in the presence of nonlinearities or non-stationary input excitations. To overcome this limitation, a novel non-parametric algorithm for automatic time-dependent modal analysis is hereby presented and discussed. This Enhanced Modal Identification for Long-term Integrity Assessment (EMILIA) algorithm can compute time-dependent estimations of the natural frequencies and mode shapes that can be critical to the early identification of hidden damage. The dynamic characterization of a beam-like structure in sound and damaged conditions is carried out for numerical validation purposes, allowing to evaluate the reliability of the proposed method over different scenarios and comparing its efficiency against traditional algorithms. Finally, further tests are conducted to analyse the sensitivity of the EMILIA algorithm to its main parameters and components.

Keywords: Time-Dependent Operational Modal Analysis, Structural Health Monitoring, Seismic Engineering, Non-Linear Structural Dynamics.

1. Introduction

Civil engineering structures and infrastructures require large investments and demand prolonged periods for their construction and commissioning [1]. Some of them are essential for modern countries and societies to support life quality, public health, security, economic growth, etc. The appropriate maintenance of such assets is therefore crucial and can significantly benefit from preventive strategies of periodic assessment [2,3] aimed at ensuring not only a satisfactory performance during the structure's lifespan but also at optimising the activities needed for diagnosis and repair after natural or man-made disasters. Structural Health Monitoring (SHM) is a field of research concerned with the development and implementation of global non-invasive techniques devoted to the condition assessment of structures. Based on different types of data collected from several kinds of sensors attached to or embedded into the structure, SHM systems offer nearly real-time information regarding structural integrity [4–6]. Though, the extraction of reliable metrics requires a preliminary application of appropriate signal processing, statistical classification and/or probability analyses to transform large, unstructured, and multi-type measured data into meaningful and accurate descriptions of the structure's health status. The SHM of civil engineering systems typically relies on ambient vibration testing methodologies, where only the structural response to unknown ambient excitations and/or random events is measured [7–9]. As widely known, this approach is suitable for any building and structure that needs to be tested continuously under operational conditions, i.e. without service interruptions. The so-called Operational Modal Analysis (OMA) strategy allows to accurately estimate parameters like modal frequencies, damping ratios and mode shapes from the sole knowledge of output acceleration measurements [10–12]. Based on the domain featured for the signal analysis, the common identification methods for OMA can be classified as frequency-domain or time-domain. Frequency-domain methods rely on Fourier's theory and the Fast Fourier Transform (FFT) [13]. Due to their ease of implementation and medium/low computational burden, they have been largely applied to the dynamic characterization of civil engineering structures [14–16]. Frequency Domain Decomposition (FDD) is currently one of the most vastly used methods [17–19]. FDD algorithm makes use of the Singular Value Decomposition (SVD) applied to the Cross Power Spectrum (CPSD) matrix of the output signals and identifies the modal parameters by selecting the frequency peaks of the power spectral densities. Further development of the method is the Enhanced Frequency Domain Decomposition (EFDD), which uses Impulse Response Functions (IRF) to enable also the estimation of the damping factor from the exponential decay of the motion amplitude [20–24]. Conversely, time-domain methods employ raw time series and do not require a space transformation to extract the modal parameters. Moreover, they demand little user interaction and present many advantages, including the possibility to estimate closely spaced modes, which are hardly distinguished by frequency domain methods. However, they are often intensive from a computational standpoint. Among them is the Stochastic Subspace Identification (SSI) method that exploits powerful time-domain Multiple Input Multiple Output (MIMO) algorithms with high immunity to signal noise. Several types of SSI methods have been proposed in the literature over the past decades, such as covariance-driven (SSI-COV), covariance-variate (SSI-CV), and data-driven (SSI-DATA). Despite the inherent differences, all these SSI methods can be generalized into a unified theory dependent on the weighting matrix selection before the parametrical decomposition [25–29].

Aiming at identifying the modal parameters of structures from output-only acceleration data, statistical methods can be employed as well. Statistic and probability-based algorithms model the structural dynamic behaviour as a time-invariant linear system resorting to polynomial data fitting, complex pole relations, and/or linear regressions. The Complex Exponential method (CE), the Least Square Complex Exponential method (LSCE), and the PolyReference Complex Exponential method (PRCE), among others, explore the relationship between the IRF and its complex poles and residues through a complex exponential and an Auto-Regressive (AR) model [30,31]. Auto-Regressive Moving-Average (ARMA) models combine two complementary polynomial regressions, an AR and a Moving Average (MA) [32]. Statistical methods have been developed for time-varying dynamic identification as well [33–35]. In [36], a time-varying autoregressive moving average model in vector form (TV-ARMAV) method for assessing linear time-varying systems is addressed. For further information on statistical methods, including applications to civil engineering systems, the reader is referred to [37–39]. Conventional modal identification procedures often fail to correctly identify structural modes when working with highly noise-contaminated measurements, nonlinear structural responses, or in the presence of vibration modes with frequencies close to a common mean, as previously mentioned [40–42]. Recent developments in the field of dynamic identification have led to the implementation of high-resolution methods, capable of detecting modal frequencies, especially closely-spaced ones, even with a low signal-to-noise ratio (high-level noise). Many of these methods as the Blind Source Separation (BSS) [43–46] or the Multiple Signal Classification (MUSIC) [47] were not originally designed for civil or seismic engineering applications, but they have been already successfully tested in many structures [48–50].

Some of the approaches previously mentioned can work with linear time-varying systems with a rate of variation lower than the period of vibration which would be enough to capture the evolution of the modal properties under environmental and operational conditions, but none of the methods discussed so far can perform modal identification with data obtained during seismic events nor represent non-linear structural behaviour. Indeed, the former can yield changes to loading scenarios and structural properties, including boundary conditions, thus affecting the intrinsic modal parameters of the system [51,52]. As previously mentioned, output-only modal identification methods, relying on a parametric decomposition applied to a weighted matrix, use the Fourier's series as solutions to the motion differential equation, thereby restricting any eigenvalue decomposition-based algorithm, like the SVD, to work with periodic and linear data. It follows that such methods are limited to the linear-elastic range of structural measurements (no-damage, no-yielding), and are not capable of performing dynamic identification in the presence of non-periodic and non-linear structural responses, failing in providing a time-dependent result. As a consequence, they cannot assess and track the evolution of the structural response while stiffness conditions are changing (e.g. during and after a strong seismic event), if not by conducting recursive or sequential analyses over time-windowed streams of data.

Several non-parametric time-frequency methods have been developed to investigate the time-dependency of modal properties. Most of the existing non-parametric algorithms were designed to assess output-only structural vibrations using exclusively an empirical approach, thereby being not suitable for Experimental Modal Analysis (EMA). Though, they have been proven successful in the context of OMA. Algorithms that sift the data by extracting time series related to the original signal waveform commonly constitute the core of such methods. For instance, the Hilbert-Huang Transform (HHT), which makes use of the Empirical Mode Decomposition (EMD) to compute pseudo-Single Degree of Freedom (SDOF) subsequences, known as Intrinsic Mode Functions (IMF) [53], has been successfully used for modal identification [54] and structural damage detection [56,57]. However, HHT cannot work with noise-contaminated data, and it hardly identifies closely located modes. Furthermore, EMD is not an orthonormal decomposition, thus, the computed IMFs may not be linearly independent functions [54,58–60]. More robust Time-Frequency Analysis (TFA) and data decomposition algorithms rely on the rock-solid Wavelet theory [61]. Wavelet Transform (WT) allows performing multi-resolution time-frequency data analysis, being capable of detecting time-dependent features even in the presence of high levels of noise. WT has become by far the most widely used time-frequency algorithm for signal processing, data denoising, and multiresolution TFA. Moreover, wavelet analysis is not only limited to assessing acceleration or displacement data for civil engineering applications, as recent researches have explored the potential of wavelets to asses time-varying entropy measurements for SHM purposes as well [62]. Further information and applications of interest can be found in [63–65]. An additional development of data-driven wavelet analysis that aims to extract IMF-like components is the Wavelet Synchro Squeezed Transform (WSST) [66]. WSST can operate both in the Fourier's and in wavelet domains and it works by first sharpening the spectrogram or wavelet scalogram through a frequency reassignment operator, then, ridge extraction techniques are employed to estimate ridges related to the instantaneous frequency behaviour. Finally, signal components are recovered by integrating the reassigned STFT or the reassigned wavelet coefficients in the vicinity of the corresponding ridges. There are also further methods that use the capability of ridge extractions applied to modal analysis. For instance, some authors have proposed instantaneous frequency identification algorithms for time-varying structures based on the ridge extraction of continuous wavelet analysis [67–69]. Nevertheless, ridge extraction methods only employ single-channel spectrogram or scalogram data, usually with high-quality signal requirements resulting in low levels of noise robustness.

Other decomposition algorithms aiming to extract IMF like components that also work in the frequency domain are the Empirical Wavelet Transform (EWT) [70] which relies on robust peak detection mechanism and spectrum segmentation techniques to develop a wavelet filter bank for effective data decomposition, the Variational Mode Decomposition (VMD) [71], and the multichannel version the Multivariate Variational Mode Decomposition (MVMD) [72] algorithm, where the MVDM is used on some of the latest developments in the frequency domain to successfully being applied to time-dependent modal analysis by short-time like approaches [73]. Both VMD and MVMD make use of adaptive Weiner filters to compute a set of modes that can properly reconstruct the system FRF.

What is stated above highlights the cogent need to move a step forward by developing new dynamic identification methods and algorithms for enhanced data analysis as well as signal processing techniques able to work in the presence of nonlinearities and noisy data, and to track the time dependency of vibration modes with reduced computational effort for real-time applications [74–77]. In this regard, the present work presents a novel non-parametric modal identification method for output-only data processing, called Enhanced Modal Identification for Long-term Integrity Assessment (EMILIA) algorithm, thoroughly described in Section 2. The proposal makes use of a discrete wavelet packet decomposition in combination with Hilbert Transform (HT) TFA. Bayesian inference is adopted to process the time-dependent information produced by more transducers simultaneously, thus providing a more reliable estimation of natural frequencies. The validation of the EMILIA algorithm is presented in Section 3 as applied research to reproduce results previously computed by traditional modal estimators using numerically simulated data. The suitability of the proposed algorithm for time-dependent modal analysis is discussed in Section 4, whereas further tests to analyse the robustness and sensitivity of the method are reported in Section 5. Finally, in Section 6, the main conclusions are drawn, and relevant future scopes are outlined.

2. Workflow description of the EMILIA algorithm

The EMILIA algorithm is composed of three main stages: (1) time-domain data decomposition; (2) time-frequency analyses; (3) statistical and probability estimations of the previously computed outputs. Each stage is conveniently detailed in the following sections. The algorithm processes raw acceleration measurements and performs dynamic identification analyses ranging from simple pointwise to full-scale MIMO. Figure 1 shows a schematic workflow of the EMILIA algorithm and its computed outcomes at each stage, using a theoretical SDOF undamped resonator with a natural frequency of 4 Hz as an example.

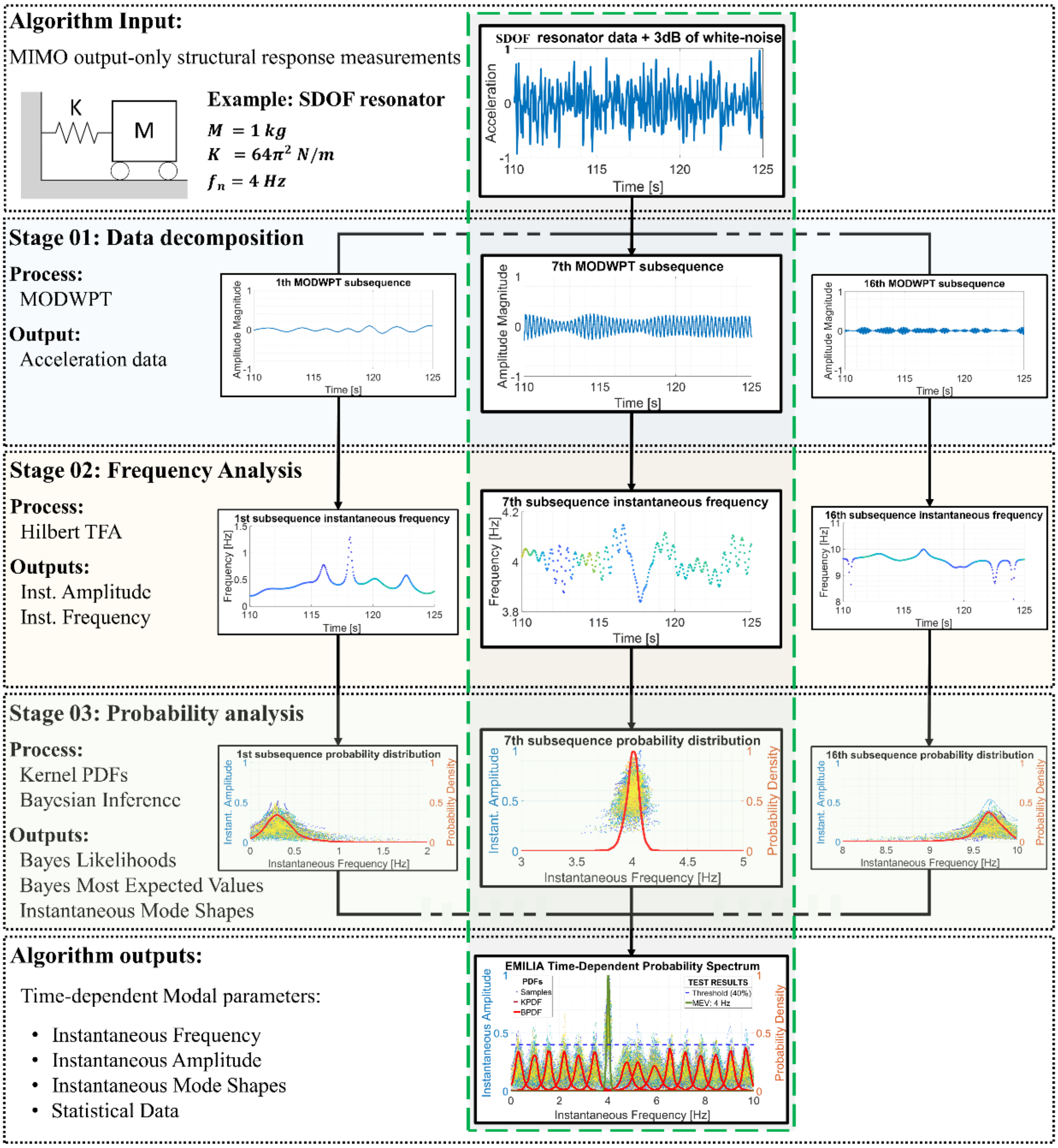

Figure 1: EMILIA algorithm workflow applied to a theoretical SDOF undamped resonator. The 1st (left side), the 7th (middle), and the 16th (right side) subsequences are presented as instances of the produced outputs. The central dashed-green-box highlights the subsequence that holds the modal Information and the outputs computed after each stage.

2.1 *Stage 01: Data decomposition*

The data decomposition stage relies on the Maximum Overlap Discrete Wavelet Packet Transform (MODWPT) algorithm to compute 2^m subsequences for each channel of the input data. Mathematically, any WT is an integral transform that represents any signal, or data stream, in terms of a set of coefficients computed through the convolution of the signal itself with dilated and translated versions of a defined mother wavelet function [61].

The Continuous Wavelet Transform (CWT) is among the most widespread methods for time-frequency data analysis, and it has been extensively applied to signal processing, data denoising, seismic and geological data analysis, image processing, etc. [78–81]. The CWT is defined as:

$$CWT\{x(t)\} = |a|^{-1/2} \int_{-\infty}^{\infty} x(t)\, \psi^* \left(\frac{t-b}{a}\right) dt \tag{1}$$

where a indicates the dilatation factor, b the translation factor, and $\psi(s)$ is the wavelet function. Despite the success of the CWT, the Discrete Wavelet Transform (DWT) represents the most used and powerful tool for studying real time-series ranging over a finite time interval through Wavelets analysis, likewise the FFT – the equivalent of the continuous Fourier Transform – in Fourier spectral analysis. In the DWT, the mother wavelet, the scaling function, and the dilatation function are discretized into a set of compactly supported functions. Thus, the DWT represents the discrete signal $x[n]$ as a time-series of coefficients computed by convolving $x[n]$ with a pair of linear filters: a low pass filter $g[n]$ as the scale function, and a high pass filter $h[n]$ as the wavelet function, where n are the discrete time-steps or samples of the digitalized data. The previous process generates two time-series of wavelet coefficients: the approximation coefficients, here denoted by $A_m[n]$ and related to the low pass filter $g_m[n]$, and the details coefficients, denoted henceforth by $D_m[n]$ and related to the high pass filter $h_m[n]$. The DWT is an orthonormal transform, thus, if an orthogonal discrete mother wavelet function is employed, the computed subsequences $A_m[n]$ and $D_m[n]$ will also be orthogonal functions.

In DWT-based decomposition algorithms, the convolution of the computed approximation coefficients with a new pair of rescaled linear low-pass and high-pass filters is repeated iteratively until reaching a certain level m, namely decomposing the signal into a set of m $D_m[n]$ and one single $A_m[n]$, through the following relations:

$$A_m[n] = (x * g)_m[t, n] = \sum_{n=1}^{N} A_{m-1}[n]\, g_m[t-n] \tag{2}$$

$$D_m[n] = (x * h)_m[t, n] = \sum_{n=1}^{N} D_{m-1}[n]\, h_m[t-n] \tag{3}$$

According to Nyquist-Shannon criteria, the original number of samples becomes redundant, thus a decimation process of $A_m[n]$ and $D_m[n]$ is performed after every level of decomposition and the high half of the frequency spectrum is discarded so that each new $A_{m+1}[n]$ and $D_{m+1}[n]$ has half the samples of its immediate preceding sequences. The decimation process restricts the maximum achievable level of decompositions M, given the number of samples N in $x[t]$, according to the expression $M = \log_2(N)$. It is worth noting that the sample size N must be an integer multiple of 2^m. Moreover, the decimation causes a loss of resolution in the low-frequency spectrum and, additionally, the discrete wavelet and scaling coefficients are not circularly shift equivariant, namely circularly shifting the time series by some amount will not circularly shift the DWT wavelet and scaling coefficients by the same amount. Lastly, the iterative halving of the number of wavelet and scaling coefficients reduces the ability to carry out statistical analyses along the coefficients.

The Discrete Wavelet Packet Transform (DWPT) is a generalization of the DWT in which, at a certain level m of the transform, the frequency spectrum is divided into 2^m equal-width segments. The m-level detail coefficients are obtained by filtering the prior-level approximation coefficients with the corresponding discrete high-pass and low-pass filters. Similar to the DWT, there is a decimation process after each level of decomposition. Increasing the decomposition level does increase the frequency resolution but, once starting with a time-series of length N, at level m there will be only $N/2^m$ DWPT coefficients for each spectrum segment. As for the Maximum Overlap Discrete Wavelet Transform (MODWT) algorithm, an undecimated decomposition iterative process is performed. In this case, the filters $h_m[n]$ and $g_m[n]$ need to be re-scaled to conserve energy. The new high-pass filter is defined as $\tilde{h}_m[n] = h_m[n]/\sqrt{2}$, and the new low-pass filter is defined as $\tilde{g}_m[n] = g_m[n]/\sqrt{2}$. The MODWT algorithm generates the MODWT wavelet coefficients and the MODWT scaling coefficients using these new filters with non-zero coefficients divided by $\sqrt{2}$. The MODWT coefficients computed at any level m are associated with the same nominal frequency band as for the DWT decomposition of the same level, though N coefficients are guaranteed at any level of the decomposition. Thus, all the computed coefficients series will have the same number of samples as the original data and further statistical analysis can be performed on the new N-length coefficients. The MODWPT [82] adopted by EMILIA is an orthonormal transform where there is no decimation process applied to the original data input, nor for any of the $W_m[n]$ subsequences computed after each level of decomposition. The most significant effect of the non-decimated decomposition process is that there is no loss of resolution on the lower part of the frequency spectrum, and similarly to the MODWT, all the computed $W_m[n]$ subsequences will keep the same number of samples as the original stream of data. Moreover, at the end of the decomposition process, the corresponding frequency spectrum will be separated in 2^m equal-width frequency bands; and, as in any orthonormal discrete Wavelet decomposition, if an orthogonal mother wavelet is used, then all the generated $W_m[n]$ subsequences will also be orthogonal functions. This first stage of the EMILIA algorithm has a $O(2m)$ time complexity according to the selected level of decomposition and the computed outcomes are two matrixes, one allocating the acceleration data and the other one allocating the displacement data. Both matrixes have a space complexity equal to $[Ch, N, 2^m]$, where Ch is the number of channels, N is the number of samples per channel in the original acceleration data, and m is the selected level of decomposition.

For any analysis, the initial level of decomposition can be set according to the Nyquist frequency. For instance, if the data from the SDOF are sampled at $f_s = 20$ Hz, the Nyquist frequency gives a total span of 10 Hz. By selecting a four-level decomposition, 2^4 subsequences will be computed out from the wavelet decomposition, enough to fully cover the frequency range with at least one subsequence per each $(f_s/2)/2^m$ spectrum segment. An unavoidable outcome of splitting the frequency spectrum in equally spaced ranges, each one of $(f_s/2)/2^m$ Hz is that some closely spaced modes may fall into a single range of the decomposition, thus, the computed component will hold more than one frequency content. As higher-order modes are commonly closer than lower ones, the identification of the fundamental modes of the system will not be compromised by this shortcoming. Still, the accurate separation of all vibration modes is always desirable and the current version of the algorithm lacks in this aspect which needs further investigations to optimise the trade-off between a sufficiently reduced span required to successfully isolate single modes and a larger span to prevent chopping the lower modes between different components or spectrum sections, without increasing excessively the computational burden that is significantly affected by the decomposition level.

Regarding the discrete wavelet function, an orthogonal mother wavelet with the highest possible amount of vanishing moments is recommended to improve the modal identification. A mother wavelet function has p vanishing moments if, and only if, the wavelet scaling function can generate polynomials up to degree $p - 1$, meaning that the scaling function alone can be used to represent such functions. Increasing the vanishing moments allows the scaling function to represent more complex functions, while reducing them limits the wavelet capability to extract periodicities, or polynomial behaviour, in a signal. A Daubechies 2 wavelet, with one vanishing moment, can easily encode polynomials of one coefficient, or constant signal components. Thus, the Daubechies 45 mother wavelet function used in the present paper can be exploited to search for polynomial functions with up to 44 coefficients, ensuring a robust modal identification, by focusing the search on strongly periodic and continuous information and overlooking random transients and stochastic components of the signal. The flowchart of Figure 1 presents the outcomes computed by a four-level MODWPT decomposition, resulting into a set of 16 acceleration subsequences. For the sake of brevity, only the first, the seventh, and the last subsequences are presented. By comparing the waveforms, it can be seen that each subsequent subsequence presents shorter periods than the previous one, containing information related to higher frequency content. The first and last subsequences are examples of lower and higher frequency spurious modes, whilst the 7th subsequence contains the actual modal information.

2.2 Stage 02: Time and frequency domain analysis

In the second stage, the HT is exploited to compute an analytical signal from each one of the subsequences produced by the MODWPT wavelet decomposition and obtain therefrom the corresponding instantaneous amplitude and instantaneous frequency data [83,84]. The HT of a discrete Gaussian white noise can produce as many different instantaneous frequency values as the number of samples of the signal. Due to the previous, broadband signals are not good candidates for Hilbert spectrum analysis and it is recommended to process, or band filter, the raw data before any further analysis in order to apply HT to mono-frequential component or pseudo-mono-frequential component signals. Hence, the application of MODWPT to decompose the acceleration data is crucial for the computation of well-behaved instantaneous frequency functions.

The HT constructs an analytical signal through the convolution of a function $x(t)$ with the function $g(t) = 1/\pi t$, according to the following formula:

$$HT\{W_m(t)\} = W_m(t) * g(t) = \frac{1}{\pi} \int_{-\infty}^{\infty} \frac{W_m(\tau)}{t-\tau}\, d\tau \tag{4}$$

The analytical signal $AS_{n,m}$ is a representation of a signal or data stream as a complex pair where the imaginary part is the HT of the real part $W_m(t)$, namely:

$$AS_m(t) = W_m(t) + iHT\{W_m(t)\} \tag{5}$$

By the modulus operation, the Instantaneous Amplitude A_{inst} is calculated as follows:

$$A_{inst}(t) = |AS_m(t)| = \sqrt{W_m(t)^2 + (HT\{W_m(t)\})^2} \tag{6}$$

Then, by the time derivative of the analytical signal´s complex angle θ_{inst_m}, the Instantaneous Frequency ω_{inst} is obtained:

$$\theta_{inst_m} = arctg\left(\frac{HT\{W_m(t)\}}{W_m(t)}\right) \tag{7}$$

$$\omega_{inst_m}(t) = \frac{\partial \theta_{inst_m}}{\partial t} \tag{8}$$

Being computed through the time derivative of the oscillatory phase, the instantaneous frequency is a time-dependent parameter.

At the output of this stage, the computed instantaneous amplitude data has a space allocation equal to $[Ch, N, 2^m]$, whilst the instantaneous frequency data has a space complexity of $[Ch, N-1, 2^m]$ (the $N-1$ number of samples of the obtained instantaneous frequency data is due to the derivation of the phase angle).

In addition to the need for well-behaved pseudo-mono-component narrow-band signals, the HT has some well-known limitations that can affect its performance as well as the computed outputs. Mainly, it is restricted by the Bedrosian and the Natter theorems [85] and can lead to outliers in the results and even negative samples of instantaneous frequencies in case of sudden changes in the input data amplitude and discontinuities. The Hilbert transform is not the only approach to compute instantaneous components from time series; several approaches have been developed especially for machinery and electrical power conditioning and maintenance, and for the signal processing fields. For instance, Direct-Quadrature (DQ) algorithms such as the Clarke-Park Transform [86] are intensively used to assess the instantaneous frequency on three-phase power systems, whereas

Discrete Energy Separation Algorithms (DESA), like the Teager-Kaiser operator [87,88] are extensively applied in speech recognition and audio analysis. Direct approaches have also been developed, like the Zero-Crossing (ZC) points-based algorithms, that analyse the number of zero-crossing points in the data in order to estimate a frequency value, but due to the nature of the calculation, the resulting value is extended to the full period of observation, producing an approximation to the instantaneous values [89,90]. Other authors have developed alternative proposals, like applying a direct ninety-degrees-shift to the data stream to extract a pseudo-analytical instantaneous phase or performing recursive normalizations of the data in order to remove the influence of the modulated amplitude on the computation of the instantaneous frequency [91]. Nevertheless, many of these algorithms remain sensitive to noise, particularly the algorithms based on cubic-splines envelopes like the Normalized Hilbert Transform (NHT) method [91], or the Teager-Kaiser operator that is particularly sensitive to wideband noise with energy levels close to or above the zero decibels [88]. Furthermore, all these methods require pseudo-mono-component-narrow-band signals as well, thus, the decomposition of the data before the calculation of the instantaneous frequency remains mandatory and of high importance. As for the proposed EMILIA algorithm, the aim is to perform modal analyses with strong motion data from seismic events, which are likely to induce non-linearities and sudden changes in the signal amplitudes and frequency content, so that it is not the burden of this stage of the algorithm to smooth the computed instantaneous frequency data, neither to remove outlier samples. According to the previous, and in order to improve the instantaneous frequency out-puts computed by the Hilbert transform adopted by the EMILIA algorithm, in the third and final stage of the proposal, Probability Density Functions (PDF) of the instantaneous frequency data are computed and Bayesian inference is applied to estimate the final outputs using for this purpose the total amount of samples available from all the channels of interest.

2.3 Stage 03: Probability analysis

In the third and final stage of the algorithm, Probability Density Functions (PDFs) of the instantaneous frequency data are computed and Bayes inference is applied to estimate the final outputs. Table 1 presents the computed variance (σ^2) and the maximum probability density of the instantaneous frequency values for the subsequences presented in Figure 1. The seventh subsequence presents a lower variance and a higher probably density peak than the other two, indicating a likely periodicity of the analysed data.

Table 1: *Maximum probability density and variance from the first, seventh, and last subsequences instantaneous frequency values.*

Subsequence	Maximum Probability	σ^2
1	2.435	0.127
7	7.160	0.004
16	2.659	24.697

In order to obtain singleton natural frequency values, the Bayesian inference is adopted by EMILIA as a method of statistical inference in which the computed probability distributions for any hypothesis (channels) are updated upon the availability of more observations (other channels) [92]. Bayes theorem is defined as:

$$P(H|O) = \frac{P(O|H) * P(H)}{P(O)} \tag{9}$$

where O is the new set of observations, H is the hypothesis whose probability may be affected by the new observations O, $P(H)$ is the estimate of the probability of the hypothesis previous to the new observations O, $P(H|O)$ is the updated probability of H given O, $P(O|H)$, also called likelihood is the probability of observing O given H, and $P(O)$ is the marginal likelihood. Computing any PDF requires the definition of an expected probability distribution to perform a parametric data fit. Normal parametric distributions are commonly chosen, nonetheless, they are not always a good fit for the probability distributions that can be found in instantaneous frequency information of structural modes.

Indeed, the latter often present resonant peaks with high amplitude and narrow bandwidth, hardly fitted by a Gaussian distribution. More details about such problems are provided in sub-section 5.2.1. To overcome this issue, non-parametrical Kernel distributions are here preferred. A Kernel distribution is a nonparametric representation of the probability distribution of a random variable, and it is defined by a smoothing function and a bandwidth value that control the smoothness of the resulting density curve. For any real values of x, the kernel density estimator is defined as:

$$\hat{f}_h(x) = \frac{1}{Nh}\sum_{n=1}^{N} K\left(\frac{x - x_n}{h}\right) \tag{10}$$

where h is the bandwidth, whereas N is the number of samples, $x_1, x_2, \dots, x_N$ are random samples from an unknown distribution and $K(\cdot)$ is the kernel smoothing function that defines the shape of the curve used to generate the computed probability distribution. Further information about Kernel distribution can be found in [93].

At the beginning of the third stage, Kernel distribution Probability Density Functions (KPDF) are computed for each one of the instantaneous frequency functions. Afterwards, the Bayes theorem is applied to calculate Bayes likelihoods (BPDF) and the singleton frequency outputs f_{MEV} through Bayes Most Expected Value (MEV).

An example of a probability spectrum computed from an SDOF undamped resonator can be seen in Figure 1. The BPDF obtained from the seventh subsequence (green continuous line) presents a peak at 4 Hz, showing a considerably higher probability than the other subsequences whose BDPFs are coloured in red. The EMILIA algorithm correctly identifies the modal information and rejects the subsequences with low probability distributions, which are likely produced by stochastic data.

As per the authors' experience, for the automatic identification of the modes, a default probability threshold equal to ten times the decomposition level is recommended.

2.4 Algorithm outputs space complexity

The final algorithm outputs are time-dependent functions carrying information about the instantaneous frequency, the instantaneous amplitude and the instantaneous displacement shapes associated with the monitored structure. The displacement mode shapes are determined through trapezoidal integration of the acceleration subsequences computed in the first stage. For the sake of clarity, it is noted that the space complexity for the ω_{inst} data is $[Ch, N-1, 2^m]$, the space complexity for the A_{inst} data is $[Ch, N, 2^m]$, and the space complexity for the Instantaneous Displacement ($\boldsymbol{\Phi}_{\mathrm{inst}}$) data is $[Ch, N, 2^m]$. At the bottom of Figure 1, an example of the final visual output that merges the frequency and amplitude information together with their evolution over time is reported. The computed ω_{inst} data are plotted against their related A_{inst}. Each sample is coloured according to a scale that allows identifying the time instant within the total duration of the acquisition. In the same graph, Bayes likelihoods are shown distinguishing with a continuous green line the identified modal information (7th subsequence with $f_{MEV} = 4$ Hz) that present a clearly higher probability density peak as compared to the other BPDFs computed from stochastic data, hereby presented with red continuous lines. For pointwise analyses, as in the example, the computed KPDFs and BPDFs coincide. However, in the case of a multichannel analysis, the differences between the computed KPDFs and the final BPDFs are relevant, as further detailed in sub-section 5.2.2.

2.5 Decomposition algorithms benchmarking test

A brief comparison of time-domain and frequency-domain decomposition algorithms is conducted to prove the selection of the MODWPT wavelet decomposition for the EMILIA algorithm. The SDOF example displayed in Figure 1 is employed for this purpose. Figure 2 shows the Hilbert spectrograms computed from three frequency-domain decompositions (HVD, EWT and VMD, on the left), and three time-domain decompositions (EMD, MODWT and MODWPT, on the right). The plots highlight the better performance of the VMD and MODWPT decomposition algorithms, as both allow a clear identification of the required information even through simple visual inspection (high-intensity data around 4 Hz). On the other hand, HVD and EMD present the worst performance by generating almost flat Hilbert spectrograms.

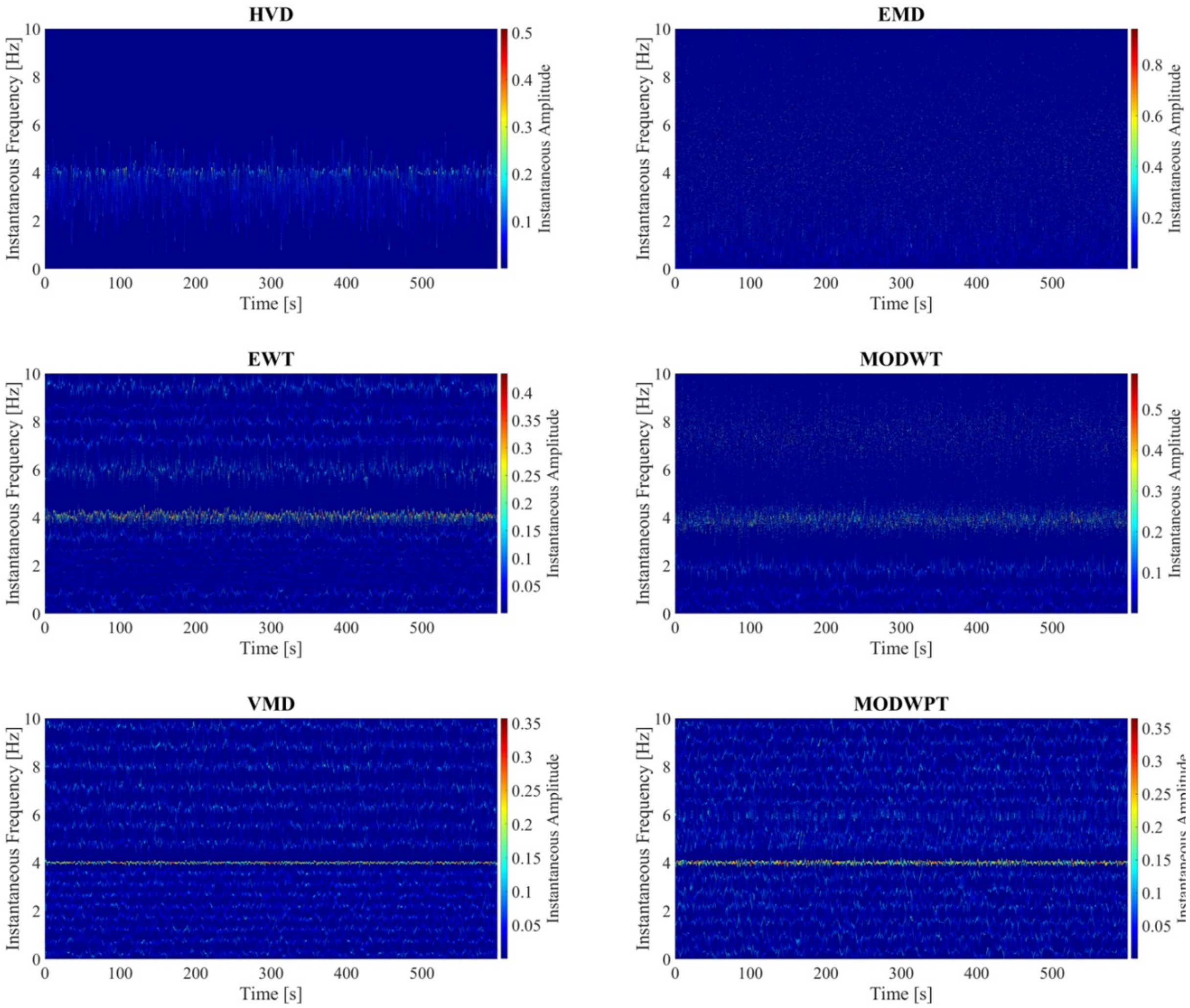

Figure 2: Comparison of Hilbert spectrograms computed with different frequency-domain decompositions (HVD, EWT, VMD) and time-domain decompositions (EMD, MODWT, MODWPT).

Table 2 summarizes some statistics from the instantaneous frequency data computed by the six decomposition algorithms. In the same table, the variance and the mean value of the instantaneous frequency computed from the component holding the modal information are also presented, corroborating the result that VMD and MODWPT decompositions lead to the best performance. For a detailed comparison between decomposition algorithms for SHM intents, the reader is referred to [94].

Table 2: Statistics computed from the instantaneous frequency data generated by the different decomposition algorithms. Data samples come from the time series containing the modal information.

	Frequency Domain			Time Domain		
Algorithm	**HVD**	**EWT**	**VMD**	**EMD**	**MODWT**	**MODWPT**
Components	7	16	16	10	5	16
f_{inst} **variance**	0.5415	0.1293	0.0015	19.8271	0.4517	0.0039
f_{inst} **mean**	3.4966	4.0050	4.0000	4.1714	3.9600	4.0000

It is worth noting that, being VMD a frequency-domain decomposition, the possibility of computing time-varying mode shapes and their higher derivatives is restricted by the same limitations as any Fourier analysis-based decomposition and, especially, by Heisenberg's uncertainty principle.

On the other hand, the MODWPT decomposition is a time-domain algorithm, hence the only requirement for the signal is to be causal. Accordingly, the MODWPT is the algorithm selected to conduct the EMILIA decomposition stage.

The application of non-parametric non-stationary signal processing methods to vibration data for modal parameter extraction in the structural field has to properly deal with features like (1) Modes located in the extreme lower part of the frequency spectrum; (2) Highly noise-contaminated signals; (3) Multiple unexpected high-transient events; (4) Structural response to ambient vibrations with very low amplitude; (5) Structural response to earthquake excitations with extreme high amplitude; (6) Measurements conducted through multi-channel setups. The EMILIA core decomposition algorithm (MODWPT) is selected because of its remarkable capabilities of performing full-resolution analysis on any part of the frequency spectrum, which means that this decomposition can work very well also in the presence of low-frequency contents as expected in the case of large structures responses. Additionally, the MODWPT algorithm performs the data decomposition in the time domain through the convolution of the scaled mother wavelet function with the signal to assess, thus ensuring great time resolution and a robust modal identification against noise-contaminated signals. Finally, as there is no decimation of the data, all the outputs have the same amount of samples, which allows performing further statistical analyses to compute the final outputs using information from all the channels.

3. Application and validation through numerical data

3.1 Case study description and preliminary analyses

The testing and validation of the algorithm presented in Section 2 are carried out through the modelling of an idealized three-span 2D bridge conducted on proprietary Finite Element (FE) analysis software [95]. The bridge features a 0.5 m thick deck supported by two square piers of 1.0 m edge and 4.5 m height, with a main span of 30 m length and two lateral spans of 14 m each (58 m long in total). For simulating the soil beneath piers and abutments, simple 1D springs are used as boundary connections in both horizontal and vertical directions. Such a structure is conceived with the intent of guaranteeing a simple yet refined baseline model to address the instantaneous dynamic identification problem without incurring into cumbersome behaviours. A schematic representation of the model is presented in Figure 3.

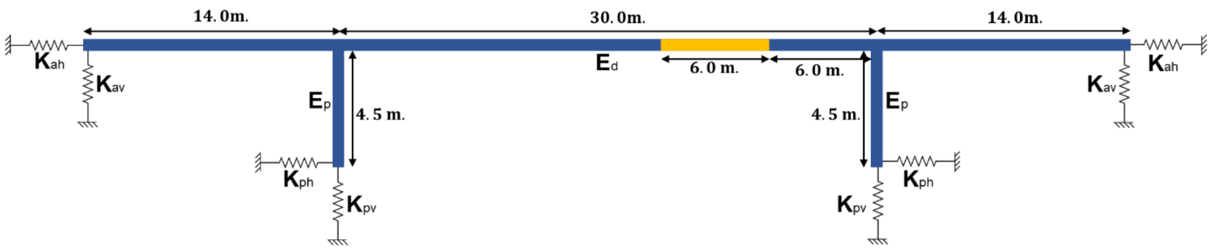

Figure 3: 2D bridge model schematic view. The damage location is highlighted in yellow.

In this "undamaged" scenario (ST00), a linear-elastic isotropic homogeneous material, with Young's modulus $E_d = 34000$ N/mm^2, Poisson's ratio $\nu_d = 0.2$ and mass density $\rho_d = 2950$ kg/m^3 is adopted for the deck (*d*), whereas a linear-elastic isotropic homogeneous material with $E_p = 22000$ N/mm^2, $\nu_p = 0.2$ and $\rho_p = 2800$ kg/m^3 is considered for the piers (*p*). Boundary spring elements located under the abutments have a stiffness equal to $K_{av} = 1.8e + 08$ N/m (vertical) and $K_{ah} = 1.8e + 08$ N/m (horizontal), while the boundary springs used under the piers feature a stiffness of $K_{pv} = 1.8e + 08$ N/m (vertical) and $K_{ph} = 2.1e + 08$ N/m (horizontal). The Rayleigh damping mass factor is equal to 1.07520 1/s and the stiffness factor is equal to 0.000734350 s. As for the mesh discretization, three-node two-dimensional beam elements of 0.25 m length - with three degrees of freedom per node, two translational and one rotational, and a quadratic order displacement interpolation - are adopted, resulting in a final model with 278 elements and 541 nodes. With the aim of investigating the EMILIA effectiveness and accuracy, two configurations with asymmetric progressive "damage" scenarios in a single location are generated by applying to a selected zone of the deck (red-coloured section of the main span in Figure 3) a stiffness reduction factor equal to 50% (ST01) and 75% (ST02) of the initial value, respectively.

A preliminary eigenvalue analysis is carried out for the bridge under the three scenarios (ST00, ST01, ST02) to obtain all the modal information necessary to drive the selection of measurement points, sampling frequency and total duration of the acquisition window for the subsequent analyses. The first ten eigenvectors and the corresponding eigenvalues are presented in Figure 4. It is observed that the first, fourth, fifth, eight and tenth eigenvectors are symmetrical vertical bending modes; the second, third, seventh, and ninth are asymmetrical vertical bending modes; whilst the sixth is a longitudinal bending mode. As expected, the number of inflexion points of the deflected bridge shapes progressively increases for higher-order frequencies with the exception of mode 4, which is a local mode involving exclusively the lateral spans.

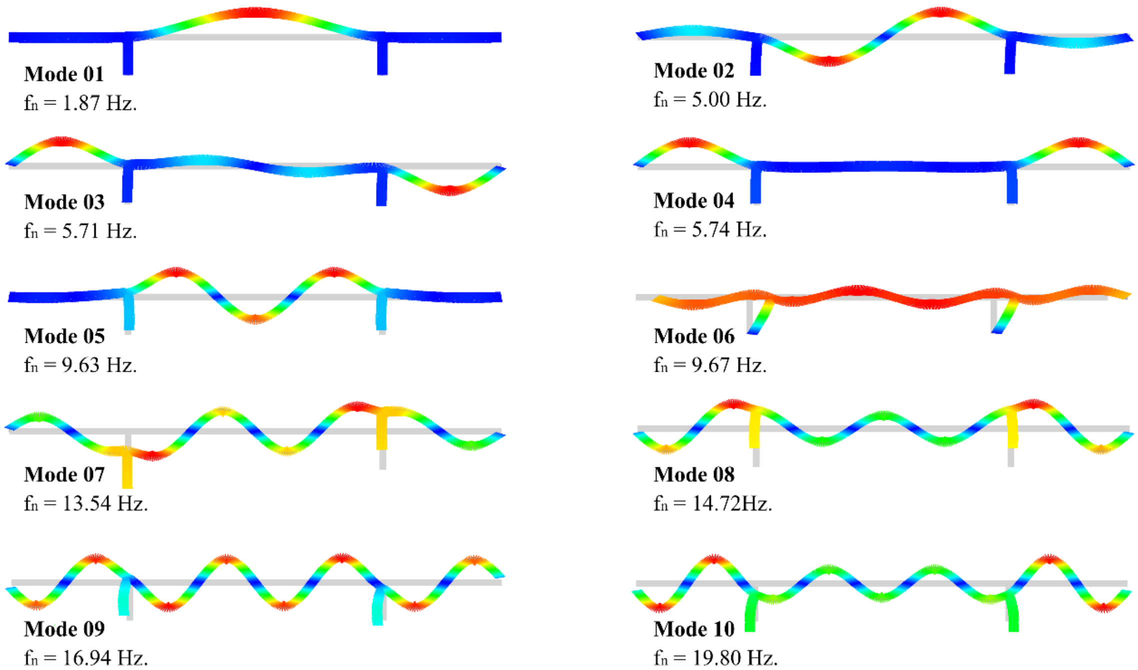

Figure 4: First ten vibration modes of the bridge computed for the ST00 stiffness configuration.

The directional effective modal masses for the same ten modes are reported in Table 3. It is noted that the modes that significantly contribute to the vibration response of the structure fall in the range 1-10 Hz.

Table 3: Eigenvalues and directional effective modal masses of the first ten numerical modes of the bridge

Mode	f_n [Hz]	Horizontal		Vertical	
		Eff. Mass [%]	Σ. Eff. Mass [%]	Eff. Mass [%]	Σ. Eff. Mass [%]
1	1.87	0.00	0.00	27.73	27.73
2	5.00	0.91	0.91	0.00	27.73
3	5.71	0.56	1.47	0.00	27.73
4	5.74	0.00	1.47	34.67	62.40
5	9.63	0.00	1.47	13.33	75.73
6	9.67	91.24	92.71	0.00	75.73
7	13.54	0.14	92.85	0.00	75.73
8	14.72	0.00	92.85	13.69	89.41
9	16.94	2.14	94.99	0.00	89.41
10	19.80	0.00	94.99	7.13	96.54

Regarding the different stiffness (or damage) scenarios, the variations of the numerical frequencies for each mode and for each stiffness configuration are reported in Table 4. In global terms, the simulated structural damage mostly affects the first, second, fifth, and ninth modes of the bridge, which feature indeed the highest frequency differences over the three stiffness configurations.

Table 4: Eigenvalues of the bridge for the three stiffness configurations (relative variation is also provided).

Mode	f_{ST00} [Hz]	f_{ST01} [Hz]	$\Delta_{00\text{-}01}$ [%]	f_{ST02} [Hz]	$\Delta_{00\text{-}02}$ [%]
1	1.87	1.81	-3.17	1.73	-7.68
2	5.00	4.57	-8.54	4.23	-15.35
3	5.71	5.70	-0.22	5.69	-0.34
4	5.74	5.74	0.01	5.74	-0.06
5	9.63	9.16	-4.85	8.48	-11.90
6	9.67	9.65	-0.23	9.62	-0.55
7	13.54	13.20	-2.53	12.66	-6.47
8	14.72	14.56	-1.09	14.39	-2.21
9	16.94	16.32	-3.69	15.64	-7.68
10	19.80	19.50	-1.52	19.17	-3.19

Linear transient analyses are also performed for each scenario by applying ten-minute random vibrations in the form of bi-directional Gaussian white-noise excitations at twenty-nine selected nodes, nineteen distributed along the main deck and five over each pier. Different random input signals sampled at 0.01 seconds (100 Hz), with peak accelerations of 0.0001 g, are considered for each node and direction. Figure 5 shows the excitation points where the input loading histories are applied (red-colour dots). The transient analyses are performed resorting to the Hilbert-Hughes-Taylor method with $\alpha = -0.1$, $\gamma = 1/2\,(1-2\alpha)$, $\beta = 1/4\,(1-\alpha)^2$, resulting in a second-order accurate and unconditionally stable integration scheme. Both the time variation of the excitation (Δ = 0.01 s) and the shortest natural period of interest of the bridge (T_6 = 0.103 s) are taken into account to choose the best time step Δt for the analysis, thus resulting in a Δt = 0.01 s. The convergence criterion is based on the energy norm with a tolerance of 0.001. Upon analysis, the nodal accelerations along X and Y are recorded at thirteen different locations (Figure 5), selected according to the significance of the modal information carried by each node in the deformed shapes of interest for the structure (e.g. higher displacements in the eigenvectors). Data are sampled at 100 Hz, thus resulting in 60.000 datapoints per channel.

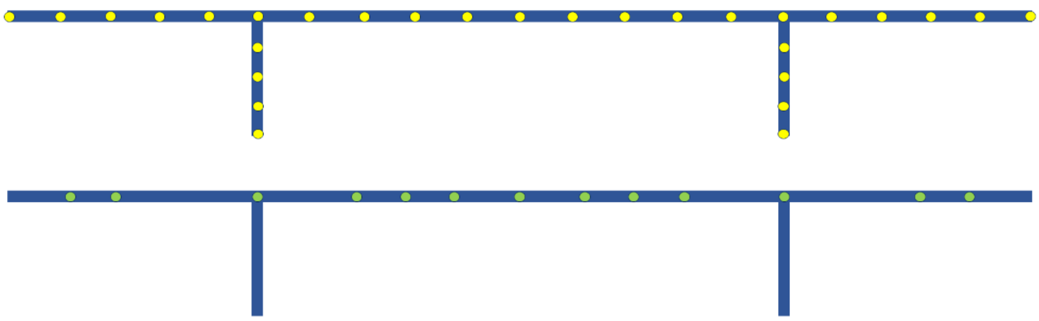

Figure 5: Distribution of the points selected for the application of random excitations (top, yellow dots). Deployment of the nodes selected for measuring the acceleration response (bottom, green dots).

3.2 *EMILIA-based dynamic identification for single scenarios*

Based on the simulated acceleration outputs, the dynamic characterization of the bridge in the three stiffness configurations is carried out by making use of two modal estimators implemented in proprietary modal analysis software [96]. i.e. the Enhanced Frequency Domain Decomposition (EFDD) and the Stochastic Subspace Identification (SSI), as well as applying the EMILIA algorithm coded in a proprietary mathematical suite [97,98]. All the input datasets use the same sampling frequency of the transient analyses and no further signal processing techniques are applied. The EMILIA algorithm produces a six-level decomposition in order to generate a total of 64 subsequences, enough to cover the complete frequency span from 0 until the Nyquist frequency (50 Hz). A Daubechies mother wavelet with 45 vanishing moments is employed, and the probability density functions are computed using the non-parametric Kernel distribution with a normal smoothing function and with a resolution of 1024 lines covering the whole frequency spectrum of interest from 0 to $f_s/2$ Hz. According to the criteria mentioned in sub-section 2.3, the probability threshold for automatic modal identification is set to ten times the decomposition level, namely to 60%. Regarding the traditional modal identification methods, the EFDD estimator presents a resolution of 1024 FFT lines with a 66% of overlap for the spectral densities estimations, whereas the SSI with the Extended Unweighted Principal Component algorithm (UPCX) adopts 100 state-space dimensions. The natural frequency results computed by EFDD, SSI-UPCX and EMILIA algorithms for the three stiffness scenarios are presented in Table 5, Table 6, and Table 7 along with the eigenvalue results of the FE model, here provided as comparative metrics to assess the EMILIA algorithm's accuracy against established estimators. The percentage errors between numerical and (simulated) experimental frequencies highlight an excellent performance of the EMILIA algorithm in terms of frequency estimations, being these in very good agreement both against the numerical counterparts and the results from the conventional output-only modal identification algorithms. It is stressed that, in order to perform an unbiased comparison and validation of the results, only the four modes successfully identified by all the modal estimators are further considered in this work. They are the first, second, third and sixth modes, hereafter referred as Mode 01, Mode 02, Mode 03 and Mode 04, respectively.

Table 5: Natural frequencies computed for the ST00 scenario with EFDD, SSI, and EMILIA algorithms.

Mode	f_{FEM} [Hz]	f_{EFDD} [Hz]	Δ [%]	f_{SSI} [Hz]	Δ [%]	f_{EMILIA} [Hz]	Δ [%]
1	1.87	1.86	-0.53	1.87	0.00	1.86	-0.53
2	5.00	4.93	-1.40	4.93	-1.40	4.93	-1.40
3	5.71	5.62	-1.58	5.62	-1.58	5.63	-1.40
4	9.67	9.13	-5.58	9.14	-5.48	9.10	-5.89

Table 6: Natural frequency values computed for the ST01 scenario with EFDD, SSI, and EMILIA algorithms.

Mode	f_{FEM} [Hz]	f_{EFDD} [Hz]	Δ [%]	f_{SSI} [Hz]	Δ [%]	f_{EMILIA} [Hz]	Δ [%]
1	1.81	1.81	0.00	1.81	0.00	1.81	0.00
2	4.57	4.52	-1.09	4.52	-1.09	4.49	-1.75
3	5.70	5.61	-1.58	5.62	-1.40	5.67	-0.53
4	9.65	9.39	-2.69	9.40	-2.59	9.38	-2.80

Table 7: Natural frequency values computed for the ST02 scenario with EFDD, SSI, and EMILIA algorithms.

Mode	f_{FEM} [Hz]	f_{EFDD} [Hz]	Δ [%]	f_{SSI} [Hz]	Δ [%]	f_{EMILIA} [Hz]	Δ [%]
1	1.73	1.72	-0.58	1.72	-0.58	1.71	-1.16
2	4.23	4.19	-0.95	4.19	-0.95	4.2	-0.71
3	5.69	5.6	-1.58	5.6	-1.58	5.63	-1.05
4	9.62	9.35	-2.81	9.16	-4.78	9.47	-1.56

Figure 6 shows the EMILIA time-dependent probability spectrum computed for the ST00. Here, the instantaneous samples are reported as dots coloured according to a scale that is a function of the time instant. These instantaneous frequency samples are computed as a time derivative of the instantaneous complex phase, and as with any complex plot, they tend to show chaotic behaviour, especially in the presence of stochastic data or sudden changes in the analysed information. In the same plot, the KPDFs of the instantaneous frequency samples are reported as red dashed lines whereas the BPDFs are either red or green continuous lines. The green continuous lines highlight the upper threshold BPDFs automatically computed for the four selected modes and whose corresponding f_{MEV} are reported in the legend; by contrast, the red continuous lines show the likelihood of rejected modes. The differences in the probability peaks between the identified modes and the rejected ones, as well as between BPDFs and KPDFs (red dashed lines) highlight the remarkable improvement in the modal identification process gained by using Bayesian inference. As all considered vibration modes fall within the frequency range 0-10 Hz, only this part of the spectra is presented. Figure 7 and Figure 8 present similar probability spectra but are computed for ST01 and ST02 configurations; for a straightforward visualization of the PDFs, the instantaneous feature variation is not presented.

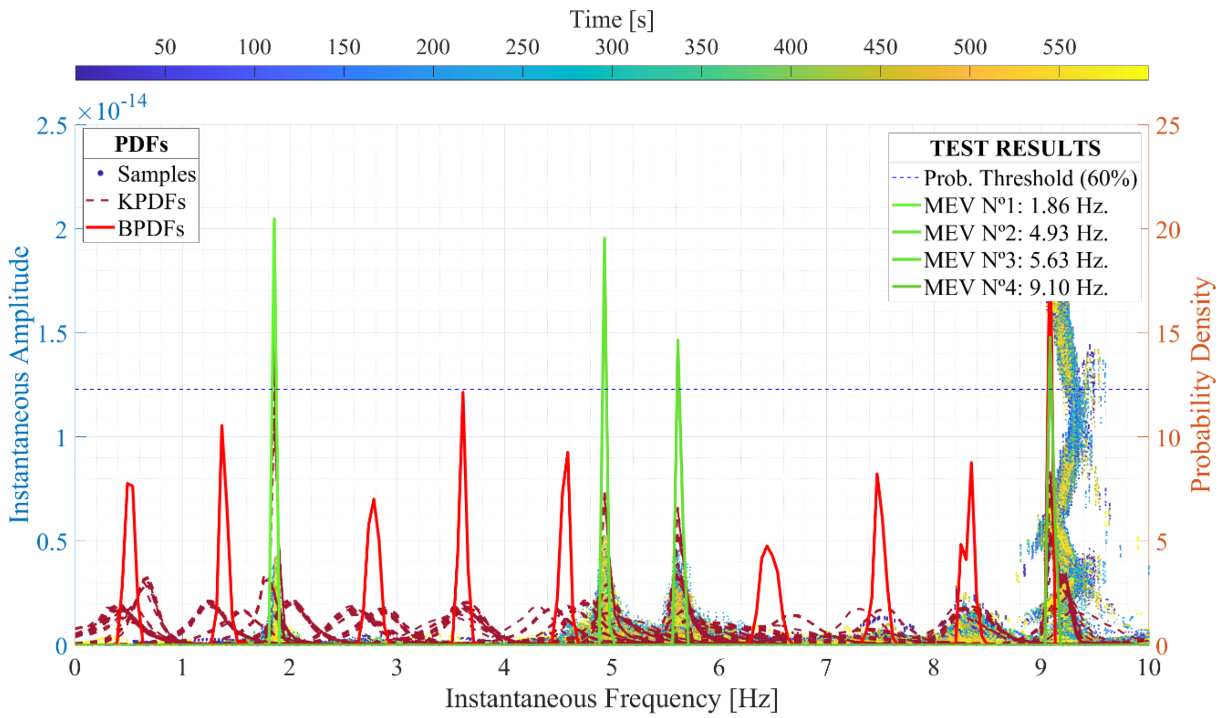

Figure 6: EMILIA time-dependent probability spectrum computed from ST00 stiffness configuration using all available channels, with a DB45 mother wavelet function and a six-level MODWPT decomposition.

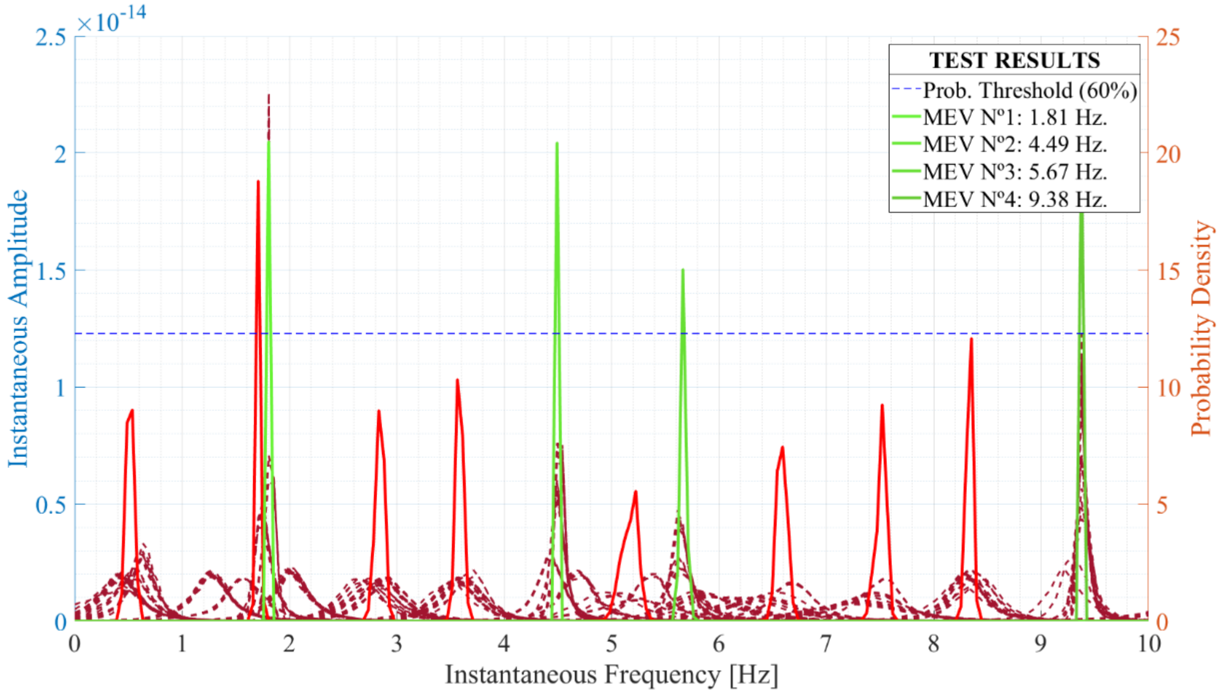

Figure 7: EMILIA probability spectrum computed from ST01 stiffness configuration using all available channels, with a DB45 mother wavelet function and a six-level MODWPT decomposition.

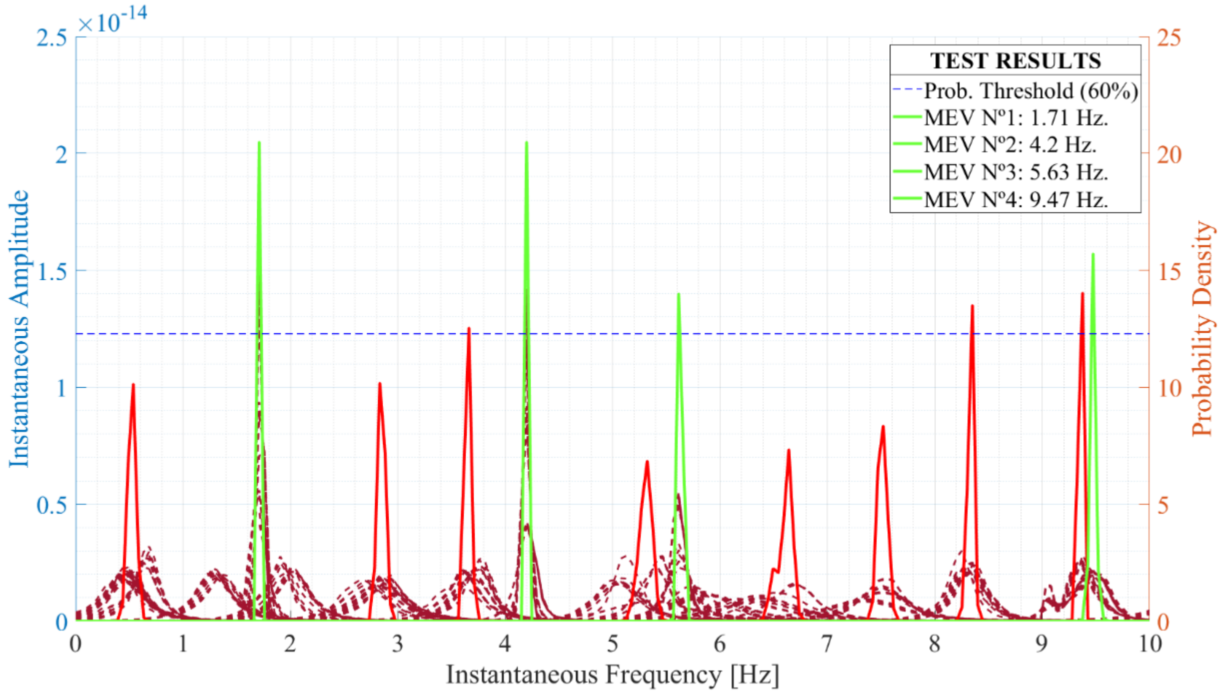

Figure 8: EMILIA probability spectrum computed from ST02 stiffness configuration using all available channels, with a DB45 mother wavelet function and a six-level MODWPT decomposition.

3.3 MAC validation for EMILIA algorithm instantaneous mode shapes

As mentioned in Section 2, one of the major strengths of the EMILIA algorithm lies in the possibility to automatically compute time-dependent outputs for every single mode, thereby yielding as many instantaneous mode shapes as the number of samples, or time-steps, of the analysed data.

To assess the accuracy of the time-varying modal displacements, the Modal Assurance Criterion (MAC) is here applied to compare each one of the instantaneous mode shapes computed by the EMILIA algorithm ("dynamic values") against the corresponding eigenvectors computed through the FE eigenvalue analysis and through the EFDD and SSI estimators ("static values").

The outputs come in the form of histograms describing the number of occurrences of the computed MAC values over the entire time window (60.000 datapoints). If no damage occurs during the acquisition of the nodal responses, instantaneous MAC values are expected to be consistently equal to or greater than 0.90, implying a correct subsequence and a positive identification of the undamaged mode shapes computed by EMILIA.

Conversely, histograms with higher amounts of instantaneous MAC values lower than 0.60 are expected if structural damage occurs during the acquisition of the vibration response of the system.

Figure 9 shows the instantaneous MAC histograms measuring the degree of consistency between the four considered mode shapes computed by the EMILIA algorithm for the ST00 stiffness configuration and the corresponding numerical eigenvectors or experimental mode shapes.

For the sake of completeness, Figure 10 gives a visual insight into all four deformed shapes of the undamaged bridge deck estimated by the EMILIA algorithm (f_1 = 1.86 Hz, f_2 = 4.93 Hz, f_3 = 5.63 Hz, f_4 = 9.10 Hz) at the instant associated with the maximum MAC value (MAC = 1) along with the evolution of the MAC histograms across the entire number of samples.

As expected, instantaneous MAC values are nearly always greater than 0.90 for all the considered modes, demonstrating the algorithm capability of not incurring into misidentifications and false positives, problems that are rather common in many standard modal identification algorithms.

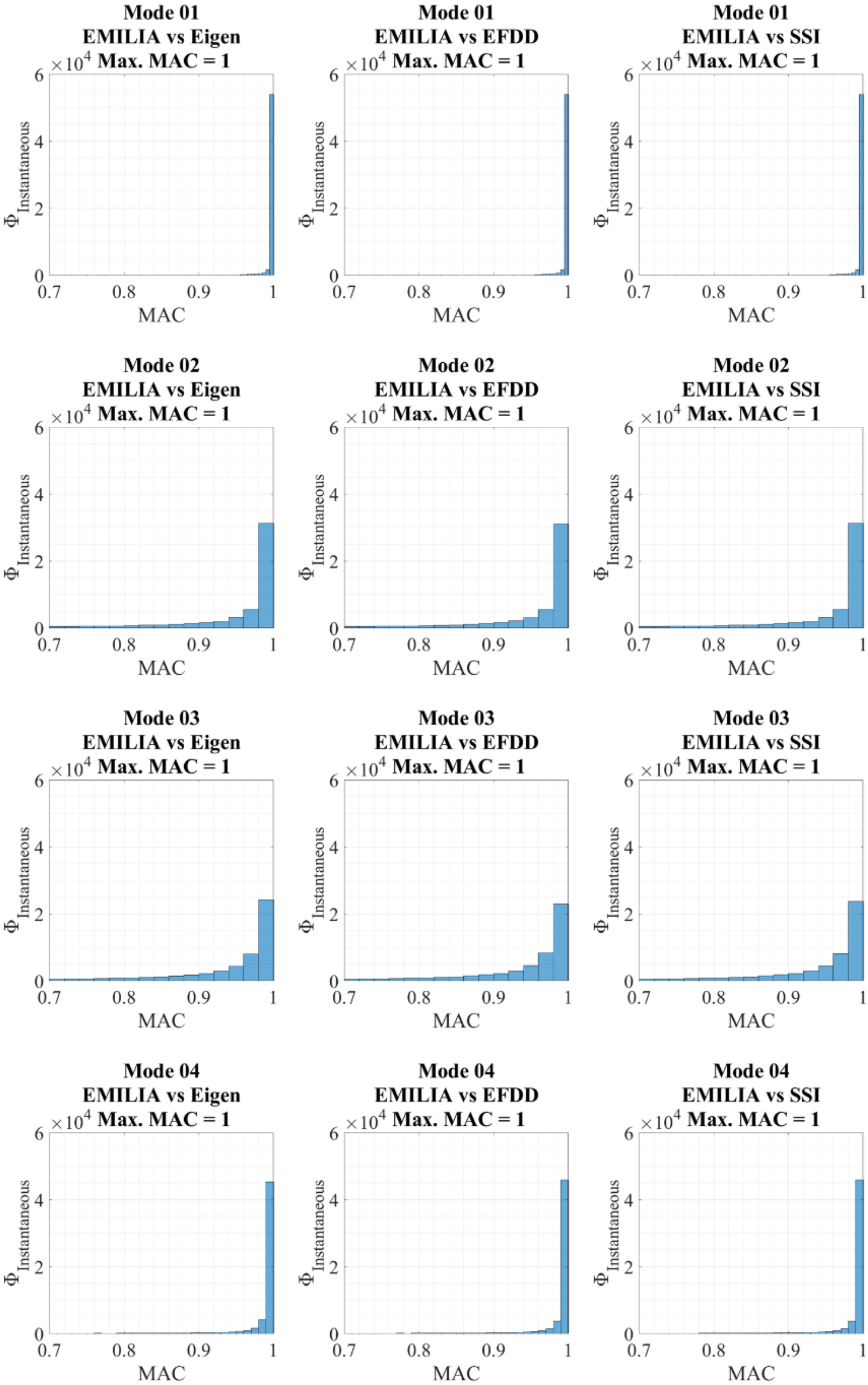

Figure 9: Instantaneous MAC results for the considered mode shapes of the undamaged bridge.

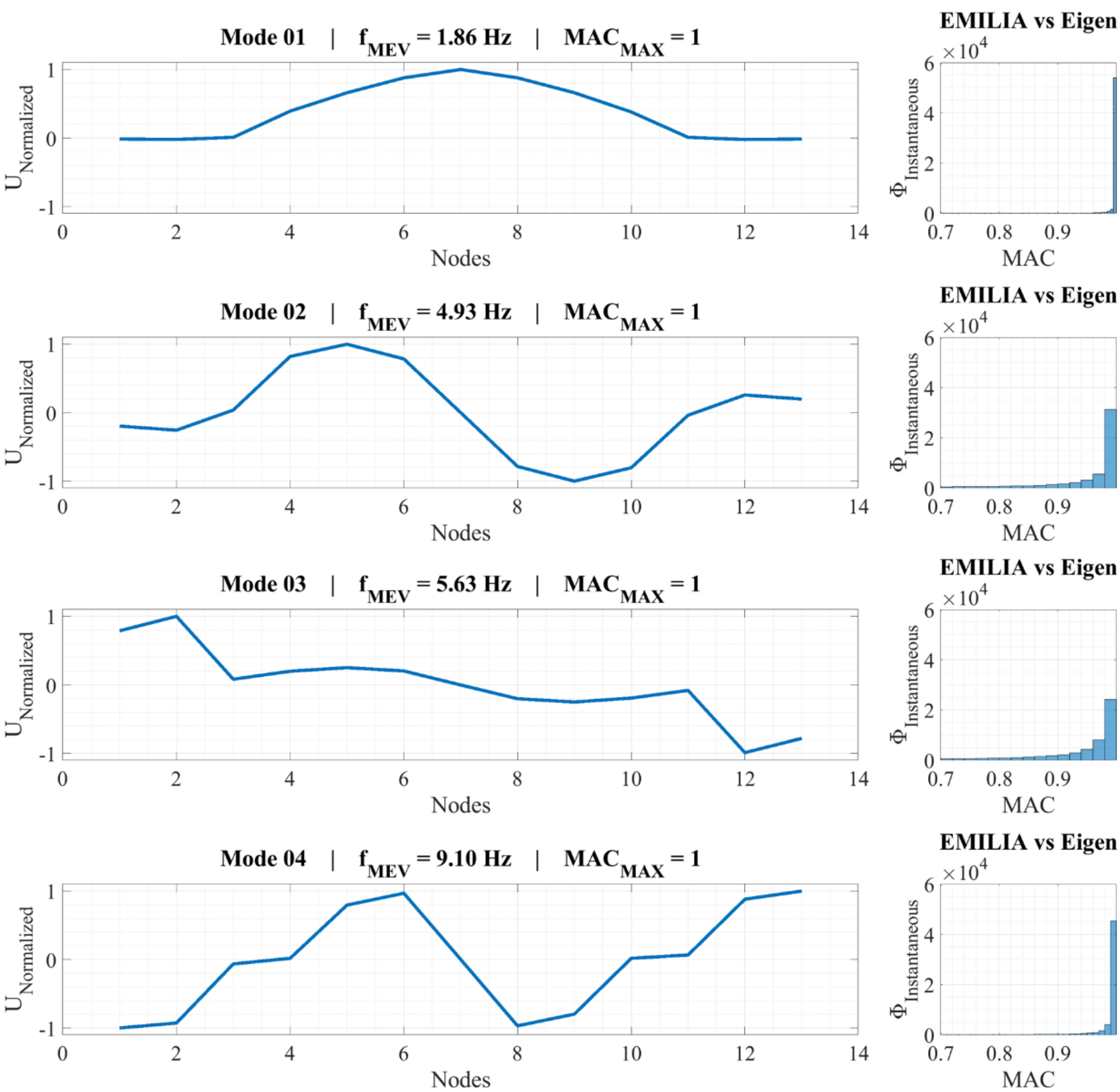

Figure 10: Mode shapes computed by the EMILIA algorithm for the ST00 configuration and relative instantaneous MAC against the numerical eigenvectors.

4. Time-dependent modal analysis across successive damage scenarios

An additional data set is built by combining the three bridge damage scenarios to generate a unique 30-minute acquisition of the 26 nodal responses (13 accelerations per direction, 180.000 datapoints per channel), suitable to be processed through the EMILIA algorithm and to be exploited for a continuous time-dependent modal analysis. The resulting trend of the instantaneous frequency values for the four modes of interest for the bridge across successive damage scenarios can be observed in Table 8.

Table 8: EMILIA frequency results and percentage difference among the three stiffness configurations.

Mode	$f_{MEVST00}$ [Hz]	$f_{MEVST01}$ [Hz]	$\Delta_{00\text{-}01}$ [%]	$f_{MEVST02}$ [Hz]	$\Delta_{00\text{-}02}$ [%]
1	1.86	1.81	-2.69	1.71	-8.06
2	4.93	4.49	-8.92	4.20	-14.81
3	5.63	5.67	0.71	5.63	≈ 0.0
4	9.10	9.38	3.08	9.47	4.07

Figure 11 shows the time-dependent probability spectrum computed using the 30-minute-long data set. The colour scale on top of the plot allows tracking both the frequency and amplitude variations of the identified modes over time, instant-by-instant.

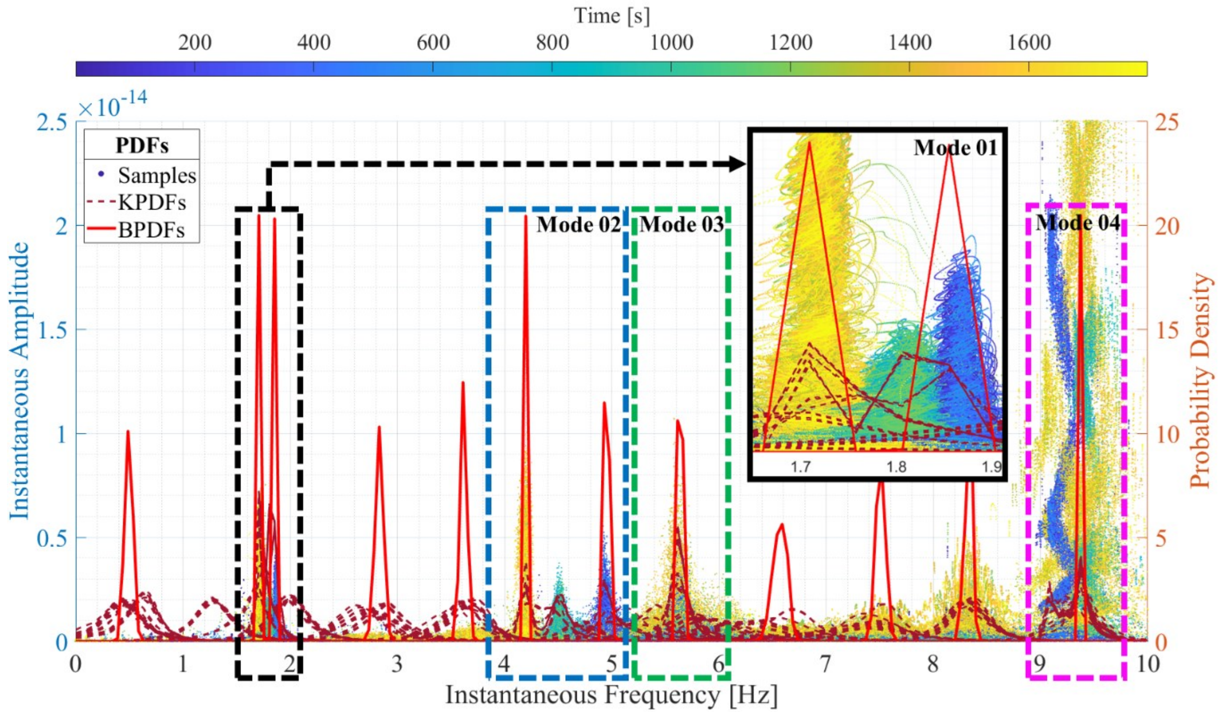

Figure 11: EMILIA time-dependent probability spectrum computed across all stiffness configurations. Close-up of the first mode's instantaneous frequency values over the three scenarios.

The EMILIA algorithm enables to follow the instantaneous frequency changes passing from the ST00 sound condition (blue samples) to the ST01 stiffness configuration (green samples) and, finally, to the ST02 stiffness configuration (yellow samples).

The close-up presented in Figure 11 provides a better insight into the changes in the instantaneous frequency values for the first mode and how EMILIA outcomes enable to follow this evolution over time, highlighting progressive frequency downshifts from f_{MEV} = 1.86 Hz (ST00, blue samples) until f_{MEV} = 1.71 Hz (ST02, yellow samples).

The blue striped line rectangle highlights the modal information about the second mode, whose instantaneous frequency values decrease from the initial f_{MEV} of 4.93 Hz, for the ST00 scenario, until the f_{MEV} of 4.20 Hz in the ST02 configuration.

Analogously, the green striped line rectangle identifies the instantaneous frequency data from the third mode. Unlike the first two modes, the third one does not undergo any sudden change in the instantaneous frequency values that remain almost constant at around 5.65 Hz throughout the acquisition window, irrespective of the new scenarios outbreak. Given the type of deflected shape featured by this mode, the insensitivity to mid-span damage was expected. A slight frequency increase is instead found for the fourth mode, highlighted in the same Figure by the pink striped line rectangle. Dealing with a longitudinal bending mode, the induced damage does not lead to an overall decrease of the global modal parameters of the bridge.

The evolution of the system's condition is further assessed by analysing the instantaneous modal displacements. Figure 12 presents, for each scenario, the deflected shapes of the four vibration modes tracked by the EMILIA algorithm, displayed in the configuration corresponding to a MAC value of 1 (numerical eigenvectors are used as reference metrics), together with the evolution of the instantaneous MAC values over the entire number of samples. The close inspection of the plots allows perceiving that the first three mode shapes experience only minor modifications upon the damage outbreak. As damage is a local phenomenon, the deflected shapes associated with global low-frequency modes are always less affected by component-wise shifts. The higher the number of inflexion points of the mode, which typically increases for higher-order frequencies, the greater the coordinate-dependent variation due to the occurrence of damage [99].

To test the capability of the EMILIA algorithm of catching possible damage-induced variations of the mode shapes during a single acquisition, further cross MAC validation is carried out considering the four FE eigenvectors estimated from the undamaged condition (ST00) as reference metrics. Progressive MAC values between EMILIA and FE mode shapes are computed in each one-second time-window, namely the maximum out of the 100 instantaneous mode shapes estimated in each second (as per the sampling frequency).

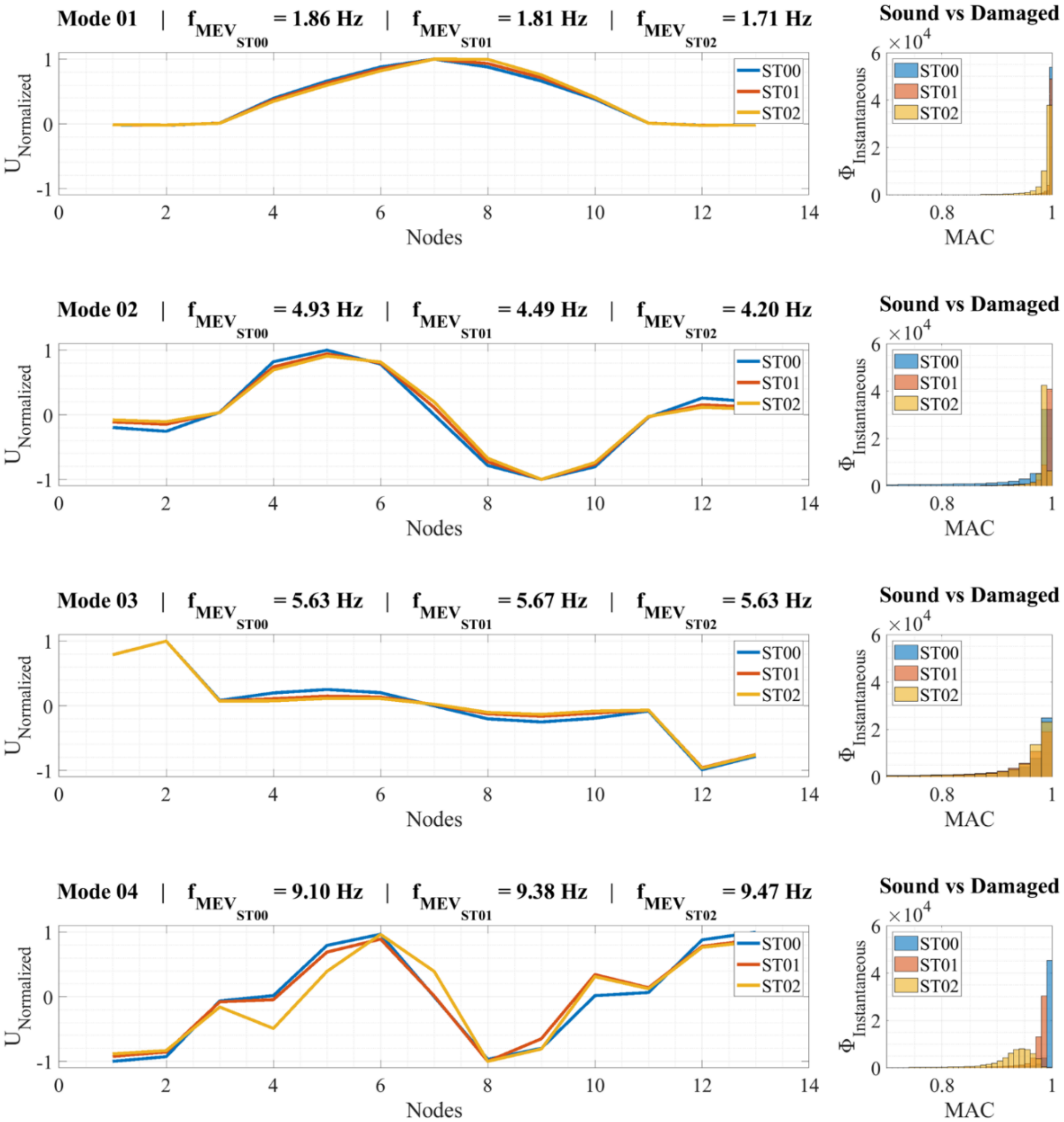

Figure 12: Evolution of the bridge mode shapes and instantaneous MAC values with progressive damage.

The obtained results are reported in Figure 13 as time-dependent MAC plots. After each damage onset, clear drops can be observed for the MAC values associated with the fourth mode and, to a minor extent, with the first and second modes. At the same time, the variance of the MAC values increases with damage across the different stiffness configurations (except for the third mode, whose MAC values remain almost constant throughout the observation time).

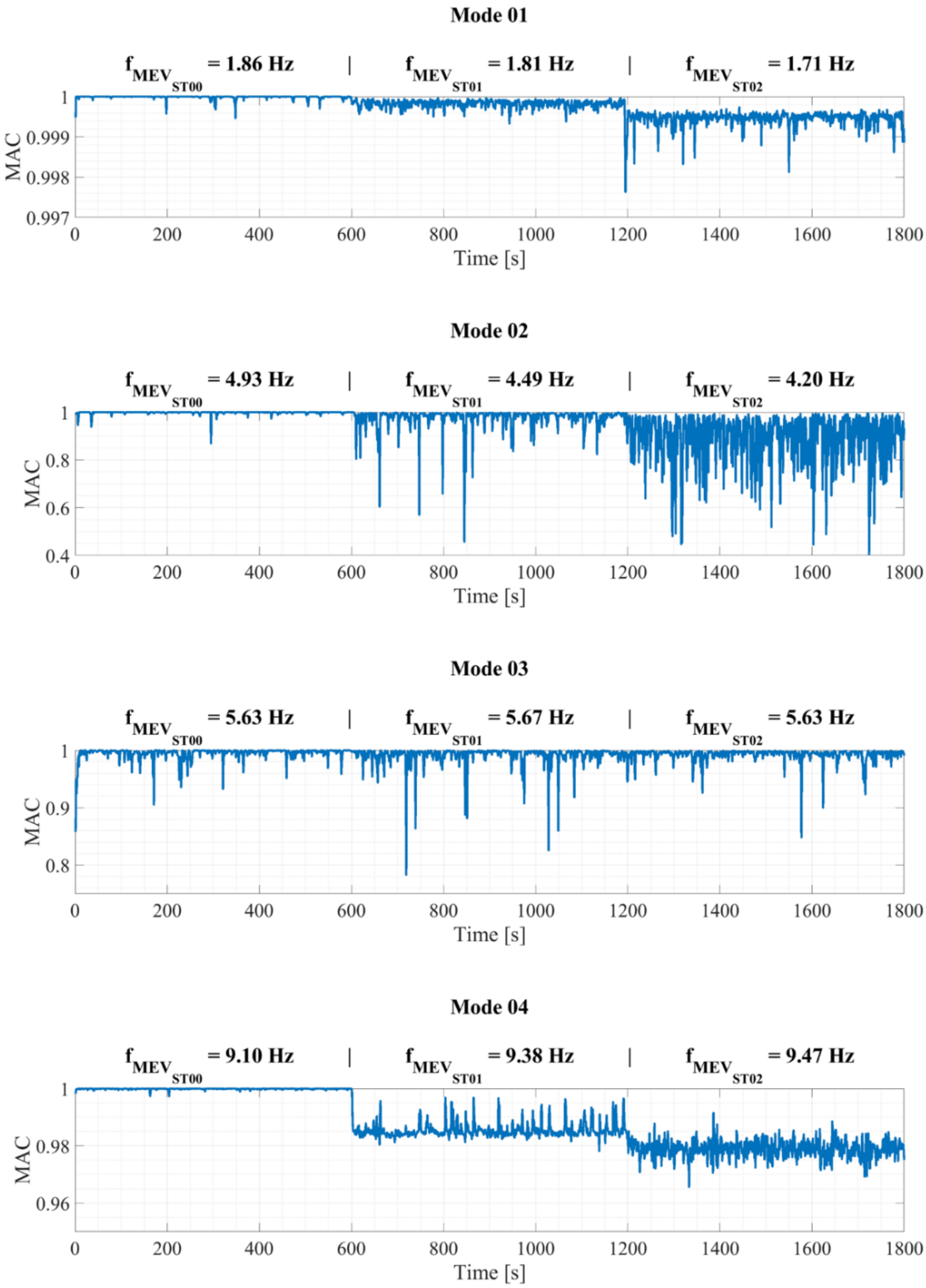

Figure 13: Evolution of the time-dependent MAC values with progressive damage for all four modes of interest.

The same time-dependent data can be also plotted in a traditional Hilbert spectrogram, aiming at identifying the precise moment of occurrence of sudden changes in the instantaneous frequency or instantaneous amplitude information. The Hilbert spectrogram associated with the first mode of the bridge is presented in Figure 14. Indeed, it is possible to locate with accuracy when the instantaneous frequency value drops after each damage onset. Although providing a better resolution in time, the Hilbert spectrum lacks information related to the probability analysis outcomes.

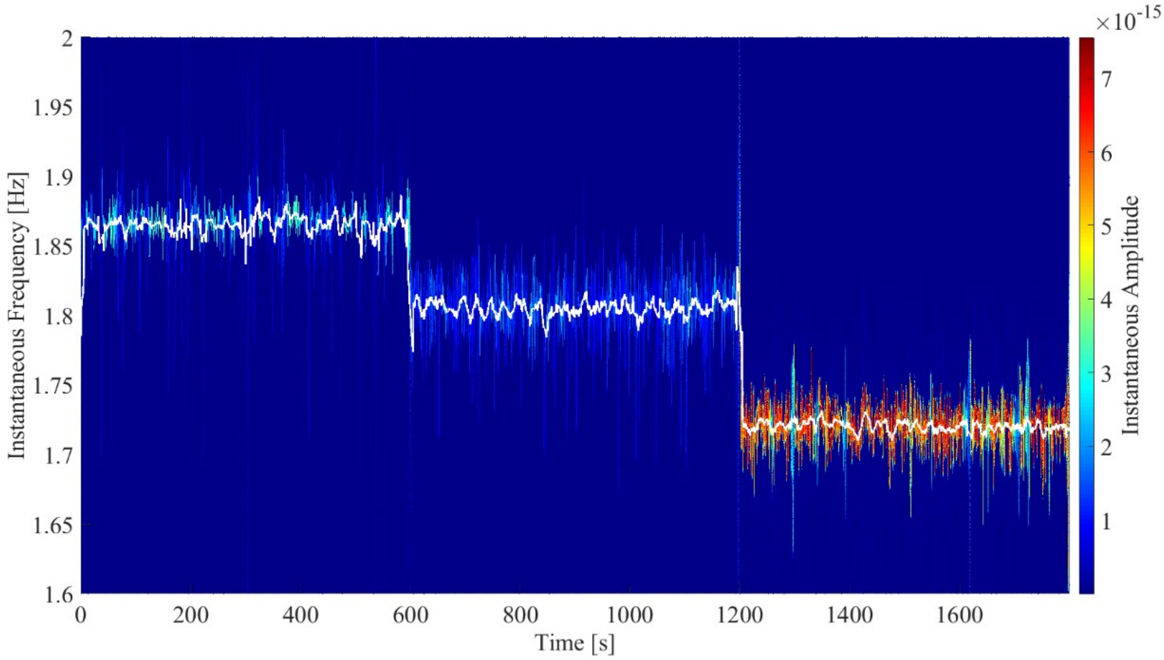

Figure 14: Hilbert spectrogram showing the first mode's instantaneous frequency evolution across the three stiffness configurations (white continuous line shows a MA of the same data).

5. Algorithm tests: parameter settings, robustness and sensitivity

Upon completion of the validation stage, additional tests are carried out to investigate the robustness and the sensitivity of EMILIA to its main parameters and processes. To this end, the same numerical case study is used to generate the needed datasets.

5.1 Decomposition level

During validation, a six-level decomposition was set according to the criteria reported in sub-section 2.1. This produced 64 subsequences from the wavelet decomposition, ensuring a good identification of the four target modes. The analyses of the ST00 dataset are here repeated considering four, six, and eight-level decompositions and using the same non-parametric Kernel distribution. According to the results reported in Table 9, by decreasing the number of decompositions below a certain level, the algorithm misses the identification of some modes, especially if they are closely spaced.

Table 9: ST00 8-level, 6-level, and 4-level Kernel results.

<table>
<tr><th rowspan="2">Modes</th><th colspan="3">8-level decomposition</th><th colspan="3">6-level decomposition</th><th colspan="3">4 -level decomposition</th></tr>
<tr><th>f_{MEV} [Hz]</th><th>σ^2</th><th>$BPDF_{max}$</th><th>f_{MEV} [Hz]</th><th>σ^2</th><th>$BPDF_{max}$</th><th>f_{MEV} [Hz]</th><th>σ^2</th><th>$BPDF_{max}$</th></tr>
<tr><td>1</td><td>1.86</td><td>≈ 0.0</td><td>20.48</td><td>1.86</td><td>≈ 0.0</td><td>20.48</td><td>1.86</td><td>≈ 0.0</td><td>20.48</td></tr>
<tr><td>2</td><td>4.93</td><td>≈ 0.0</td><td>20.48</td><td>4.93</td><td>≈ 0.0</td><td>19.55</td><td rowspan="2">5.04</td><td rowspan="2">0.004</td><td rowspan="2">8.96</td></tr>
<tr><td>3</td><td>5.62</td><td>≈ 0.0</td><td>20.48</td><td>5.63</td><td>≈ 0.0</td><td>14.65</td></tr>
<tr><td>4</td><td>9.23</td><td>≈ 0.0</td><td>20.48</td><td>9.10</td><td>≈ 0.0</td><td>14.8</td><td>9.08</td><td>≈ 0.0</td><td>20.48</td></tr>
</table>

For instance, the four-level decomposition produces only 16 subsequences, not enough to properly cover the 50 Hz frequency span. Thus, the algorithm outputs for the second and third modes are mixed (highlighted in light grey in Table 9), showing considerably lower probabilities and higher variance than for the six-level decomposition results. On the other hand, increasing the number of decompositions leads to higher peaks in the computed BPDFs but, after a certain level, with little improvement of the modal identification accuracy.

Selecting a large number of decomposition levels is not worth the increment in computational burden (namely computation time and memory requirements). Yet, at the beginning of any modal analysis process using the EMILIA algorithm, it is fundamental to establish the initial level of decomposition by checking the frequency span to be analysed and the required frequency resolution. Indeed, the resolution depends on the space between the modes which is rarely known a-priori.

According to what is mentioned in sub-section 2.1, for a sampling rate between 20 Hz and 50 Hz, choosing a decomposition level between three and five is a good starting point that produces between eight and thirty-two subsequences. Similarly, for a sampling rate between 50 Hz and 400 Hz, a four-level to eight-level decompositions would provide between 16 and 256 subsequences, respectively.

With these suggested decomposition levels, and according to the relation $(f_s/2)/2^m$, choosing a four-level decomposition for analysing data sampled at 40 Hz will produce 16 spectrum segments, each one with an equal span of 1.25 Hz; while choosing a six-level decomposition for data sampled at 100 Hz will produce 64 spectrum segments with an equal length of 0.83 Hz each one. Undersetting the decomposition level will produce longer spectrum spans, thus affecting the accuracy of the identification and increasing the probabilities of mixing too closely located modes.

Increasing the MODWPT decomposition level does increase the number of computed subsequences, thus, the number of segments in which the frequency spectrum will be divided (increased frequency resolution). However, using extremely high decomposition levels produces an enormous amount of KPDFs and BPDFs placed really close along the frequency spectrum, with a massive increase in the computational burden. It is worth mentioning that the algorithm has a geometric *O(2m)* time complexity related to the decomposition level, and the space complexity of the outputs is also affected by the same complexity. Moreover, increasing the level likely flattens the probability spectrum, hindering the modal identification. Therefore, a correct setting of the decomposition level is paramount and finding a good trade-off between resolution and computational burden may require a case-specific preliminary modal analysis.

5.2 *Probability analyses settings and configurations*

5.2.1 *Effects of varying the PDF distribution: Nonparametric vs Parametric*

During the validation, the dynamic identification was carried out by relying on the non-parametric Kernel distribution. This distribution is arguably the best fit for instantaneous frequency information. This can be seen in Figure 15, where PDFs computed resorting to Kernel non-parametric probability distributions (red lines) are compared against PDFs computed using Gaussian normal probability distributions (blue lines).

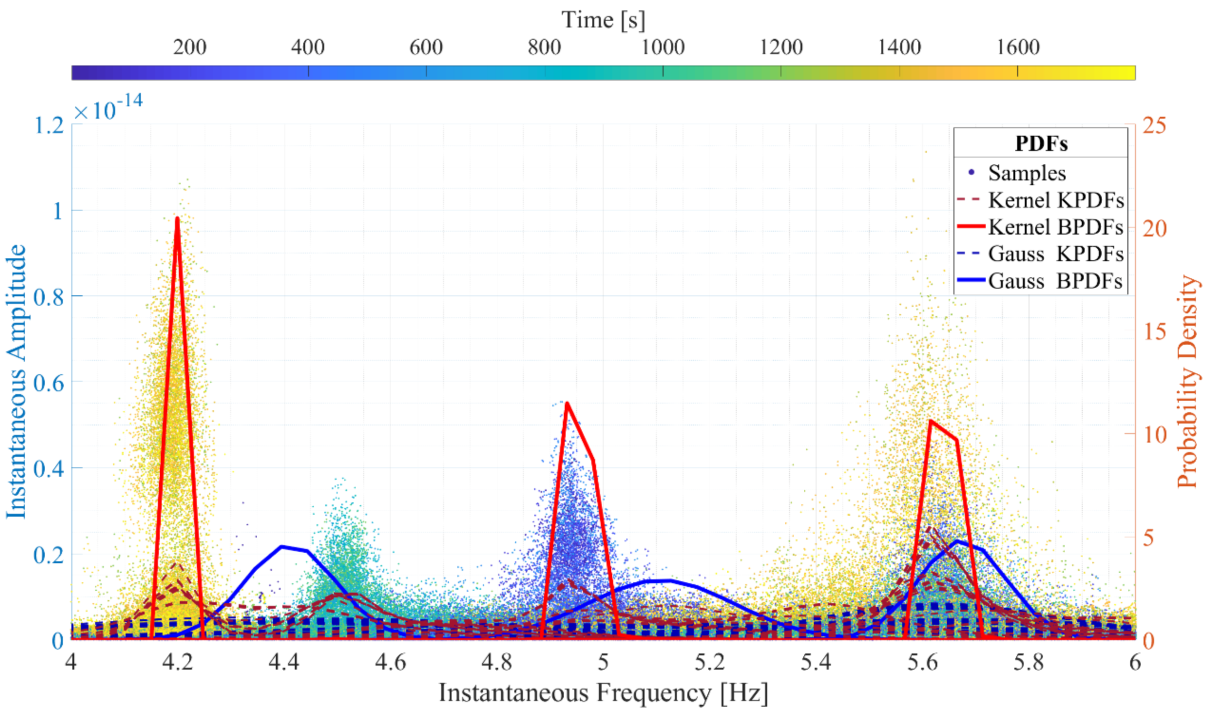

Figure 15: EMILIA probability spectrum showing the probability analyses outputs computed by using a Gaussian parametric distribution (blue lines), and by using a Kernel non-parametric distribution (red lines).

Here, the 30-minute combined scenarios data set is considered, and as expected, the lower peaks of each PDF computed with the Gaussian distribution are considerably evident. This, in turn, hinders the automatic identification when Gaussian distribution is used, since the lower peaks fail to overcome the threshold set to ten-times the decomposition level (60%). Finally, the estimation produced through Bayesian inference applied to the Gaussian PDFs presents a lower accuracy in terms of frequency values, which further deteriorates when assessing non-linear data.

5.2.2 Bayes Inference for computing final outcomes

EMILIA algorithm features a final stage based on Bayesian inference to ensure a better and more accurate calculation of the natural frequencies with respect to the commonly adopted frequentist approach that directly computes the mean of the maximum probability values from each KPDF. For instance, Figure 16 on the left shows the EMILIA output for the first mode in the sound condition scenario (ST00) computed with a resolution of 1024 FFT lines. This is the first bending mode; therefore, it presents higher modal displacements at mid-span. The exact frequency value is 1.87 Hz. The red striped lines in Figure 16 show the KPDFs, while the computed BPDFs are plotted in red continuous line. Comparing the estimated frequency values reported in the left plot legend, it is clear how using Bayes inference gives more accurate results (f_{MEV} = 1.86 Hz) than the simple average of all KPDFs maximum probability values (f_{AVG} = 1.94 Hz). Such results can be explained by analysing the distributions computed from each channel data: the KPDFs with higher probabilities are computed from nodes located at mid-span, while the KPDFs with lower probability peaks are from the nodes located along the side spans. These latter KPDFs are shifted over the frequency spectrum, with respect to the former, leading to a lower accuracy of their mean. Bayesian inference, instead, weights the estimation based on each measurement point by the computed distribution densities, therefore, higher peaks contribute more to the final BPDF.

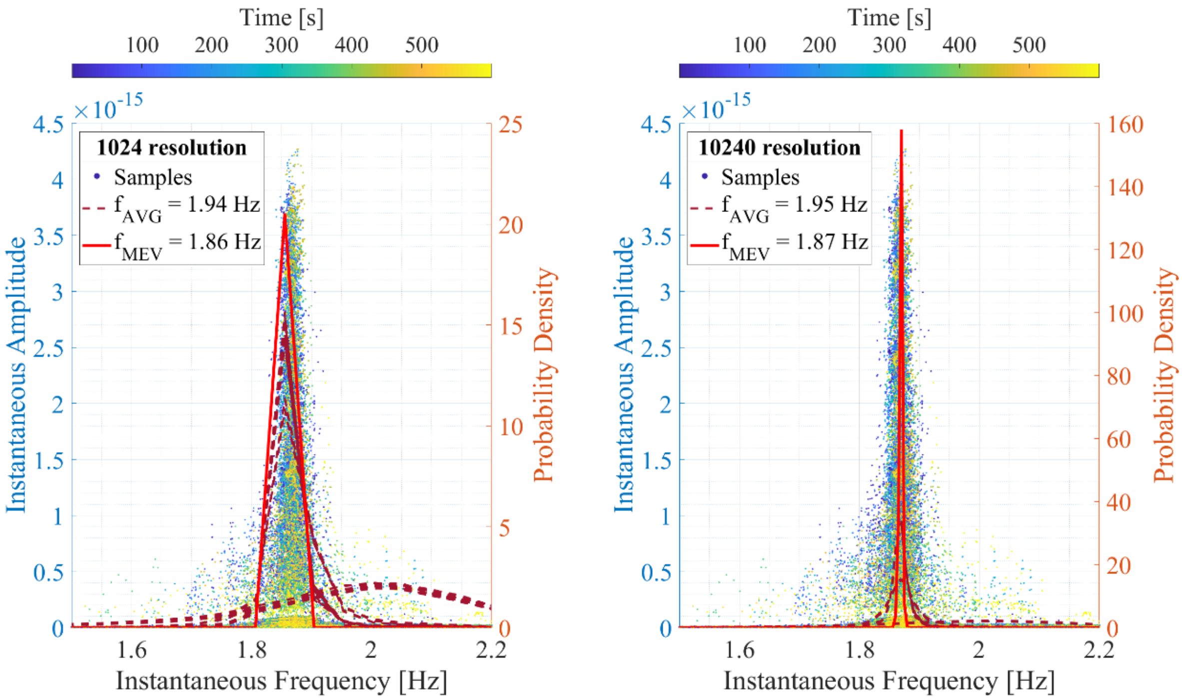

Figure 16: Mode 1 Kernel PDFs and Bayesian PDFs computed using data from the ST00 stiffness configuration. For the left plot PDFs computation, a resolution of 1024 FFT lines is used; whilst for the right plot, a resolution of 10240 FFT lines is used.

5.2.3 PDFs frequency resolution setting

Similar to the decomposition level, the PDFs frequency resolution is an intrinsic parameter of the EMILIA algorithm, which may affect its performance both in terms of accuracy and computational burden. Increasing the frequency resolution, indeed, generates better fits and smoothest distributions, likely increasing the accuracy of the computed natural frequencies as well. For instance, Figure 16 at right shows a time-dependent probability spectrum computed from the first mode data of the ST00 scenario using 10240 lines of resolution for all the KPDFs and the subsequent BPDFs.

Comparing this spectrum with the one in the left plot, where the default 1024 lines are used, it is noted that the distributions present higher amplitude and narrower bandwidth, with an overall improved estimation performance, considering the exact frequency value of 1.87 Hz. However, this almost negligible increment in the accuracy of the result (0.53%) requires a considerable increment of the computational burden, both in the time needed to complete the analysis and in the size of the output files. Moreover, the f_{MEV} results converge to the one presented in Figure 16's right-plot legend by using a resolution of 4069 lines, and they remain almost constant until 32768 lines of resolution (no further analyses with higher resolution were computed). Therefore, commonly used resolutions of 512 to 2048 lines can be used as a good initial setting. Case-specific analyses might be carried out to optimise the parameter setting.

6. Conclusions

In the present work, a novel non-parametric algorithm for automatic time-dependent modal identification was presented and validated over the simulated structural response of a three-span bridge, comparing the results against well-known traditional modal estimators (i.e. EFDD and SSI-UPCX). The proposed EMILIA algorithm successfully identified the modal parameters of the system in its undamaged and damaged conditions, where the latter was obtained by applying a progressive stiffness reduction factor to a selected area of the deck. The algorithm allowed the processing of data generated by combining in a single simulated acquisition the records from different structural conditions, leading to time-dependent outputs. From the analyses performed, the following conclusions can be drawn:

- The combination of WT and HT produces an effective mean for decomposing, processing and assessing structural data. MODWPT decomposition can deal with high noise-contaminated data and can precisely separate MIMO vibration measurements into a set of orthogonal time-dependent subsequences, where each subsequence is a pseudo-SDOF spectral component. As broadband signals are not good candidates for HT analysis, and as ambient structural vibration measurements have the deterministic information well-hidden between stochastic data, the MODWPT decomposition is of critical importance to successfully apply the HT to analyse structural vibrations due to ambient excitations and finally compute well behaved time-dependent instantaneous frequency and instantaneous amplitude functions. Furthermore, WT and HT are not limited by the superposition principle, and they can properly extract time and frequency information on non-linear and non-periodic data, thus they can be used to assess temporal changes in the structural response, even with measurements recorded during seismic or other exceptional events.
- Using probability analysis to compute the algorithm outputs improves the accuracy and the performance of the EMILIA algorithm. When dealing with time-varying data, parametric distributions may cause misidentifications and deteriorate the estimation accuracy. Therefore, a Kernel non-parametric probability distribution was employed to fit the instantaneous frequency data produced by each measurement point. Finally, by applying Bayesian inference to the KPDFs the accuracy in the estimation of the natural frequencies is further enhanced, irrespective of the number of channels used and the location of the sensors in the structure.
- For long-term structural assessment, the time-dependent outputs, namely the instantaneous frequency values and instantaneous mode shapes, allow to directly perform further signal processing and statistical analyses for SHM and damage identification purposes. In particular, the EMILIA algorithm was able to correctly track the evolution over time of the case study frequencies and mode shapes, including their damage-induced shifts, demonstrating potential beneficial use as a tool for prompt damage detection during seismic events.

- The time-dependent modal features that can be considered resorting to an EMILIA-driven dynamic identification are not limited to instantaneous frequencies and displacement mode shapes, but also mode shape derivatives (e.g. slopes and curvatures) can be computed as time-dependent functions. This capability of the EMILIA algorithm to compute time-dependent outputs and to track the temporal evolution of the modal parameters certainly represents an added value for SHM, especially for rapid structural integrity assessments, as the proposed tool can be successfully employed for online structural monitoring and damage identification, safely driving rescue operations during emergency phases.
- A shortcoming of the current configuration of the algorithm is regarding the hurdle to separating closely spaced modes that are located in the same frequency span, especially when there are big differences in the complexity of the modes. Large civil structures can usually be characterised by the assessment of the first two or three pairs of bending modes, in addition to the first pair of torsional modes, all of them generally located on the lower part of the frequency spectrum, thus, the EMILIA algorithm is designed to mainly work with low frequencies. The previous will have as an outcome the previously mentioned impossibility to separate closely spaced modes located inside the same frequency span, which will affect especially the higher modes.

Other aspects that deserve in-depth investigations are the capabilities of the algorithm to properly extract and render the nonlinearities of time-variant structural responses, in addition to assessing the robustness of the algorithm to deal with uncorrelated noise contamination. To this end, additional analyses for a comprehensive assessment of the proposed method are under development making use of nonlinear time-dependent data from more realistic cases of study subjected to progressive seismic-induced stiffness reductions. Lastly, further exploring EMILIA time-dependent modal outputs and associated derivatives as damage-sensitive features for online and nearly real-time early warning is, indeed, the ultimate target of the research.

CRediT authorship contribution statement

Manuel F. Hormazabal: Investigation, Writing-Original draft preparation, Software, Formal Analysis, Visualization. **Alberto Barontini:** Validation, Writing-Reviewing and Editing. **Maria G. Masciotta:** Conceptualization, Methodology, Writing-Reviewing and Editing. **Daniel V. Oliveira:** Supervision, Writing-Reviewing and Editing.

Declaration of Interest

The authors declare that they have no known competing financial interests or personal relationships that could have appeared to influence the work reported in this paper.

Acknowledgements

This work was funded by the Chilean National Agency for Research and Development (ANID), through the programme "Doctorado en el Extranjero Becas Chile, Convocatoria 2020" [PhD abroad grants programme, Becas Chile, call 2020], Folio – 72204431 [Sheet number – 72210443]. This work was partly financed by FCT/MCTES through national funds (PIDDAC) under the R&D Unit Institute for Sustainability and Innovation in Structural Engineering (ISISE), under reference UIDB/04029/2020.

References

[1] P. Thoft-Christensen, Infrastructures and life-cycle cost-benefit analysis, Structure and Infrastructure Engineering. 8 (2012) 507–516. https://doi.org/10.1080/15732479.2010.539070.
[2] S. Kim, D.M. Frangopol, Cost-Effective Lifetime Structural Health Monitoring Based on Availability, Journal of Structural Engineering. 137 (2011) 22–33. https://doi.org/10.1061/(ASCE)ST.1943-541X.0000280.

[3] A.J. Hughes, R.J. Barthorpe, N. Dervilis, C.R. Farrar, K. Worden, A probabilistic risk-based decision framework for structural health monitoring, Mech Syst Signal Process. 150 (2021) 107339. https://doi.org/10.1016/j.ymssp.2020.107339.
[4] Vistasp M. Karbhari, Farhad Ansari, eds., Structural health monitoring of civil infrastructure systems, 1st ed., Woodhead Publishing, Cambridge, 2009.
[5] M.-G. Masciotta, J.C.A. Roque, L.F. Ramos, P.B. Lourenço, A multidisciplinary approach to assess the health state of heritage structures: The case study of the Church of Monastery of Jerónimos in Lisbon, Constr Build Mater. 116 (2016) 169–187. https://doi.org/10.1016/j.conbuildmat.2016.04.146.
[6] M.P. Limongelli, M. Çelebi, eds., Seismic Structural Health Monitoring. From Theory to Successful Applications., 1st ed., Springer, 2019.
[7] C. Zhang, A.A. Mousavi, S.F. Masri, G. Gholipour, K. Yan, X. Li, Vibration feature extraction using signal processing techniques for structural health monitoring: A review, Mech Syst Signal Process. 177 (2022) 109175. https://doi.org/10.1016/j.ymssp.2022.109175.
[8] S. Das, P. Saha, S.K. Patro, Vibration-based damage detection techniques used for health monitoring of structures: a review, J Civ Struct Health Monit. 6 (2016) 477–507. https://doi.org/10.1007/s13349-016-0168-5.
[9] F. Ubertini, G. Comanducci, N. Cavalagli, Vibration-based structural health monitoring of a historic bell-tower using output-only measurements and multivariate statistical analysis, Struct Health Monit. 15 (2016) 438–457. https://doi.org/10.1177/1475921716643948.
[10] R. Brincker, Some Elements of Operational Modal Analysis, Shock and Vibration. 2014 (2014) 11. https://doi.org/http://dx.doi.org/10.1155/2014/325839.
[11] L.F. Ramos, L. Marques, P.B. Lourenço, G. de Roeck, A. Campos-Costa, J. Roque, Monitoring historical masonry structures with operational modal analysis: Two case studies, Mech Syst Signal Process. 24 (2010) 1291–1305. https://doi.org/10.1016/j.ymssp.2010.01.011.
[12] C. Rainieri, G. Fabbrocino, Operational Modal Analysis of Civil Engineering Structures, 1st ed., Springer New York, New York, NY, 2014. https://doi.org/10.1007/978-1-4939-0767-0.
[13] M. Frigo, S.G. Johnson, The Design and Implementation of FFTW3, Proceedings of the IEEE. 93 (2005) 216–231. https://doi.org/10.1109/JPROC.2004.840301.
[14] C.S. Oliveira, M. Navarro, Fundamental periods of vibration of RC buildings in Portugal from in-situ experimental and numerical techniques, Bulletin of Earthquake Engineering. 8 (2010) 609–642. https://doi.org/10.1007/s10518-009-9162-1.
[15] X. Hu, B. Wang, H. Ji, A Wireless Sensor Network-Based Structural Health Monitoring System for Highway Bridges, Computer-Aided Civil and Infrastructure Engineering. 28 (2013) 193–209. https://doi.org/10.1111/j.1467-8667.2012.00781.x.
[16] M. Valla, P. Gueguen, B. Augère, D. Goular, M. Perrault, Remote Modal Study of Reinforced Concrete Buildings Using a Multipath Lidar Vibrometer, Journal of Structural Engineering. 141 (2015) 1–10. https://doi.org/10.1061/(ASCE)ST.1943-541X.0001087.
[17] R. Brincker, C.E.; Ventura, P. Andersen, Damping Estimation by Frequency Domain Decomposition, in: Proceedings of IMAC 19 : A Conference on Structural Dynamics, Society for Experimental Mechanics, Kissimmee, 2001: pp. 698–703.
[18] R. Brincker, L. Zhang, P. Andersen, Modal Identification from Ambient Responses using Frequency Domain Decomposition, in: IMAC 18 : Proceedings of the International Modal Analysis Conference (IMAC), San Antonio, 2000: pp. 625–630.
[19] R. Brincker, L. Zhang, P. Andersen, Modal identification of output-only systems using frequency domain decomposition, Smart Mater Struct. 10 (2001) 441–445. https://doi.org/10.1088/0964-1726/10/3/303.
[20] J. Rodrigues, R. Brincker, Application of the Random Decrement Technique in Operational Modal Analysis, in: Proceedings of the 1st International Operational Modal Analysis Conference, Aalborg Universitet, København, 2005: pp. 191–200.
[21] J. Rodrigues, R. Brincker, P. Andersen, Improvement of frequency domain output-only modal identification from the application of the random decrement technique, in: Proceedings of IMAC22 : A Conference on Structural Dynamics, Society for Experimental Mechanics, Dearborn, 2004: pp. 92–100.

[22] F. Magalhães, Á. Cunha, E. Caetano, R. Brincker, Damping estimation using free decays and ambient vibration tests, Mech Syst Signal Process. 24 (2010) 1274–1290. https://doi.org/10.1016/j.ymssp.2009.02.011.

[23] R. Brincker, P. Andersen, N.-J. Jacobsen, Automated Frequency Domain Decomposition for Operational Modal Analysis, in: Conference Proceedings : IMAC-XXIV: A Conference & Exposition on Structural Dynamics, Society for Experimental Mechanics, Orlando, 2007: pp. 1–7.

[24] R. Brincker, L. Zhang, Frequency domain decomposition revisited, in: Proceedings of the 3rd International Operational Modal Analysis Conference - IOMAC, Starrylink Editrice, Portonovo, Italy, 2009: pp. 615–626.

[25] B. Peeters, G. de Roeck, Stochastic System Identification for Operational Modal Analysis: A Review, J Dyn Syst Meas Control. 123 (2001) 659–667. https://doi.org/10.1115/1.1410370.

[26] M. Döhler, P. Andersen, L. Mevel, Operational Modal Analysis Using a Fast Stochastic Subspace Identification Method, in: Conference Proceedings of the Society for Experimental Mechanics Series, 2012: pp. 19–24. https://doi.org/10.1007/978-1-4614-2425-3_3.

[27] M. Döhler, P. Andersen, L. Mevel, Variance computation of modal parameter estimates from UPC subspace identification, in: IOMAC - 7th International Operational Modal Analysis Conference, Ingolstadt, Germany, 2017. https://hal.inria.fr/hal-01522137.

[28] S. Gres, M.D. Ulriksen, M. Döhler, R.J. Johansen, P. Andersen, L. Damkilde, S.A. Nielsen, Statistical methods for damage detection applied to civil structures, Procedia Eng. 199 (2017) 1919–1924. https://doi.org/10.1016/j.proeng.2017.09.280.

[29] S. Greś, M. Döhler, P. Andersen, L. Mevel, Kalman filter-based subspace identification for operational modal analysis under unmeasured periodic excitation, Mech Syst Signal Process. 146 (2021) 106996. https://doi.org/10.1016/j.ymssp.2020.106996.

[30] D.L. Brown, R.J. Allemang, R. Zimmerman, M. Mergeay, Parameter Estimation Techniques for Modal Analysis, in: SAE Transactions, 1979: pp. 828–846. https://doi.org/10.4271/790221.

[31] H. Vold, J. Kundrat, G.T. Rocklin, R. Russell, A Multi-Input Modal Estimation Algorithm for Mini-Computers, in: SAE Technical Paper, USA, 1982: pp. 67–77. https://doi.org/10.4271/820194.

[32] W. Gersch, Estimation of the autoregressive parameters of a mixed autoregressive moving-average time series, IEEE Trans Automat Contr. 15 (1970) 583–588. https://doi.org/10.1109/TAC.1970.1099560.

[33] Y. Grenier, Time-dependent ARMA modeling of nonstationary signals, IEEE Trans Acoust. 31 (1983) 899–911. https://doi.org/10.1109/TASSP.1983.1164152.

[34] K. Kostoglou, M. Lunglmayr, Root tracking using time-varying autoregressive moving average models and sigma-point Kalman filters, EURASIP J Adv Signal Process. 2020 (2020) 6. https://doi.org/10.1186/s13634-020-00666-7.

[35] S.-D. Zhou, W. Heylen, P. Sas, L. Liu, Parametric modal identification of time-varying structures and the validation approach of modal parameters, Mech Syst Signal Process. 47 (2014) 94–119. https://doi.org/10.1016/j.ymssp.2013.07.021.

[36] M. Bertha, J.-C. Golinval, Identification of non-stationary dynamical systems using multivariate ARMA models, Mech Syst Signal Process. 88 (2017) 166–179. https://doi.org/10.1016/j.ymssp.2016.11.024.

[37] H.C. Gomez, H.S. Ulusoy, M.Q. Feng, Variation of modal parameters of a highway bridge extracted from six earthquake records, Earthq Eng Struct Dyn. 42 (2013) 565–579. https://doi.org/10.1002/eqe.2227.

[38] M. Gong, J. Sun, L. Xie, Identification of model structure parameters via combination of AFMM and ARX from seismic response data, Earthquake Engineering and Engineering Vibration. 13 (2014) 411–423. https://doi.org/10.1007/s11803-014-0252-y.

[39] T. Saito, J.L. Beck, Bayesian model selection for ARX models and its application to structural health monitoring, Earthq Eng Struct Dyn. 39 (2010) 1737–1759. https://doi.org/10.1002/eqe.1006.

[40] R. Pintelon, P. Guillaume, J. Schoukens, Uncertainty calculation in (operational) modal analysis, Mech Syst Signal Process. 21 (2007) 2359–2373. https://doi.org/10.1016/j.ymssp.2006.11.007.

[41] X.X. Bao, C.L. Li, C.B. Xiong, Noise elimination algorithm for modal analysis, Appl Phys Lett. 107 (2015) 041901. https://doi.org/10.1063/1.4927642.

[42] S.-K. Au, J.M.W. Brownjohn, J.E. Mottershead, Quantifying and managing uncertainty in operational modal analysis, Mech Syst Signal Process. 102 (2018) 139–157. https://doi.org/10.1016/j.ymssp.2017.09.017.

[43] G. Kerschen, F. Poncelet, J.-C. Golinval, Physical interpretation of independent component analysis in structural dynamics, Mech Syst Signal Process. 21 (2007) 1561–1575. https://doi.org/10.1016/j.ymssp.2006.07.009.

[44] F. Poncelet, G. Kerschen, J.-C. Golinval, D. Verhelst, Output-only modal analysis using blind source separation techniques, Mech Syst Signal Process. 21 (2007) 2335–2358. https://doi.org/10.1016/j.ymssp.2006.12.005.

[45] B. Hazra, A. Sadhu, A.J. Roffel, S. Narasimhan, Hybrid Time-Frequency Blind Source Separation Towards Ambient System Identification of Structures, Computer-Aided Civil and Infrastructure Engineering. 27 (2012) 314–332. https://doi.org/10.1111/j.1467-8667.2011.00732.x.

[46] K. Yang, K. Yu, Q. Li, Modal parameter extraction based on Hilbert transform and complex independent component analysis with reference, Mech Syst Signal Process. 40 (2013) 257–268. https://doi.org/10.1016/j.ymssp.2013.05.003.

[47] R. Schmidt, Multiple emitter location and signal parameter estimation, IEEE Trans Antennas Propag. 34 (1986) 276–280. https://doi.org/10.1109/TAP.1986.1143830.

[48] X. Jiang, H. Adeli, Pseudospectra, MUSIC, and dynamic wavelet neural network for damage detection of highrise buildings, Int J Numer Methods Eng. 71 (2007) 606–629. https://doi.org/10.1002/nme.1964.

[49] J.P. Amezquita-Sanchez, A. Garcia-Perez, R.J. Romero-Troncoso, R.A. Osornio-Rios, G. Herrera-Ruiz, High-resolution spectral-analysis for identifying the natural modes of a truss-type structure by means of vibrations, Journal of Vibration and Control. 19 (2013) 2347–2356. https://doi.org/10.1177/1077546312456228.

[50] R.A. Osornio-Rios, J.P. Amezquita-Sanchez, R.J. Romero-Troncoso, A. Garcia-Perez, MUSIC-ANN Analysis for Locating Structural Damages in a Truss-Type Structure by Means of Vibrations, Computer-Aided Civil and Infrastructure Engineering. 27 (2012) 687–698. https://doi.org/10.1111/j.1467-8667.2012.00777.x.

[51] Y. Xia, B. Chen, S. Weng, Y.-Q. Ni, Y.-L. Xu, Temperature effect on vibration properties of civil structures: a literature review and case studies, J Civ Struct Health Monit. 2 (2012) 29–46. https://doi.org/10.1007/s13349-011-0015-7.

[52] H. Uebayashi, M. Nagano, T. Hida, T. Tanuma, M. Yasui, S. Sakai, Evaluation of the structural damage of high-rise reinforced concrete buildings using ambient vibrations recorded before and after damage, Earthq Eng Struct Dyn. 45 (2016) 213–228. https://doi.org/10.1002/eqe.2624.

[53] N.E. Huang, Z. Shen, S.R. Long, M.C. Wu, H.H. Shih, Q. Zheng, N.-C. Yen, C.C. Tung, H.H. Liu, The empirical mode decomposition and the Hilbert spectrum for nonlinear and non-stationary time series analysis, Proceedings of the Royal Society of London. Series A: Mathematical, Physical and Engineering Sciences. 454 (1998) 903–995. https://doi.org/10.1098/rspa.1998.0193.

[54] W. Shi, J. Shan, X. Lu, Modal identification of Shanghai World Financial Center both from free and ambient vibration response, Eng Struct. 36 (2012) 14–26. https://doi.org/10.1016/j.engstruct.2011.11.025.

[55] E. Simon Carbajo, R. Simon Carbajo, C. Mc Goldrick, B. Basu, ASDAH: An automated structural change detection algorithm based on the Hilbert–Huang transform, Mech Syst Signal Process. 47 (2014) 78–93. https://doi.org/10.1016/j.ymssp.2013.06.010.

[56] J.N. Yang, Y. Lei, S. Lin, N. Huang, Hilbert-Huang Based Approach for Structural Damage Detection, J Eng Mech. 130 (2004) 85–95. https://doi.org/10.1061/(ASCE)0733-9399(2004)130:1(85).

[57] Z.K. Peng, P.W. Tse, F.L. Chu, An improved Hilbert–Huang transform and its application in vibration signal analysis, J Sound Vib. 286 (2005) 187–205. https://doi.org/10.1016/j.jsv.2004.10.005.

[58] N.E. Huang, Z. Wu, A review on Hilbert-Huang transform: Method and its applications to geophysical studies, Reviews of Geophysics. 46 (2008) RG2006. https://doi.org/10.1029/2007RG000228.
[59] N.E. Huang, S.S.P. Shen, Hilbert-Huang Transform and Its Applications, WORLD SCIENTIFIC, 2005. https://doi.org/10.1142/5862.
[60] I. Daubechies, Ten Lectures on Wavelets, Society for Industrial and Applied Mathematics, 1992. https://doi.org/10.1137/1.9781611970104.
[61] M. Civera, C. Surace, The Instantaneous Spectral Entropy for Real-time, Online Structural Health Monitoring., J Phys Conf Ser. 2184 (2022) 012033. https://doi.org/10.1088/1742-6596/2184/1/012033.
[62] M. Ruzzene, A. Fasana, L. Garibaldi, B. Piombo, Natural Frequencies And Dampings Identification Using Wavelet Transform: Application To Real Data, Mech Syst Signal Process. 11 (1997) 207–218. https://doi.org/10.1006/mssp.1996.0078.
[63] H. Dai, G. Xue, W. Wang, An Adaptive Wavelet Frame Neural Network Method for Efficient Reliability Analysis, Computer-Aided Civil and Infrastructure Engineering. 29 (2014) 801–814. https://doi.org/10.1111/mice.12117.
[64] M. Hormazábal, M. Masciotta, D. Oliveira, Proposal for a Time-Dependent Dynamic Identification Algorithm for Structural Health Monitoring, in: 12th International Conference on Structural Analysis of Historical Constructions, CIMNE, 2021. https://doi.org/10.23967/sahc.2021.196.
[65] I. Daubechies, J. Lu, H.-T. Wu, Synchrosqueezed wavelet transforms: An empirical mode decomposition-like tool, Appl Comput Harmon Anal. 30 (2011) 243–261. https://doi.org/10.1016/j.acha.2010.08.002.
[66] K. Dziedziech, W.J. Staszewski, T. Uhl, Wavelet-based modal analysis for time-variant systems, Mech Syst Signal Process. 50–51 (2015) 323–337. https://doi.org/10.1016/j.ymssp.2014.05.003.
[67] C. Wang, W.-X. Ren, Z.-C. Wang, H.-P. Zhu, Instantaneous frequency identification of time-varying structures by continuous wavelet transform, Eng Struct. 52 (2013) 17–25. https://doi.org/10.1016/j.engstruct.2013.02.006.
[68] D. Iatsenko, P.V.E. McClintock, A. Stefanovska, Extraction of instantaneous frequencies from ridges in time-frequency representations of signals, Signal Processing. 125 (2016) 290–303. https://doi.org/10.1016/j.sigpro.2016.01.024.
[69] J. Gilles, Empirical Wavelet Transform, IEEE Transactions on Signal Processing. 61 (2013) 3999–4010. https://doi.org/10.1109/TSP.2013.2265222.
[70] K. Dragomiretskiy, D. Zosso, Variational mode decomposition, IEEE Transactions on Signal Processing. 62 (2014) 531–544. https://doi.org/10.1109/TSP.2013.2288675.
[71] N. ur Rehman, H. Aftab, Multivariate Variational Mode Decomposition, IEEE Transactions on Signal Processing. 67 (2019) 6039–6052. https://doi.org/10.1109/TSP.2019.2951223.
[72] S. Liu, R. Zhao, K. Yu, B. Liao, B. Zheng, A novel real-time modal analysis method for operational time-varying structural systems based on short-time extension of multivariate VMD, Structures. 37 (2022) 389–402. https://doi.org/10.1016/j.istruc.2021.12.070.
[73] F. Ubertini, C. Gentile, A.L. Materazzi, Automated modal identification in operational conditions and its application to bridges, Eng Struct. 46 (2013) 264–278. https://doi.org/10.1016/j.engstruct.2012.07.031.
[74] M.G. Masciotta, Damage Identification of Structures based on Spectral Output Signals, University of Minho, 2015.
[75] M.-G. Masciotta, L.F. Ramos, P.B. Lourenço, M. Vasta, Spectral algorithm for non-destructive damage localisation: Application to an ancient masonry arch model, Mech Syst Signal Process. 84 (2017) 286–307. https://doi.org/10.1016/j.ymssp.2016.06.034.
[76] M.-G. Masciotta, L.F. Ramos, P.B. Lourenço, M. Vasta, G. de Roeck, A spectrum-driven damage identification technique: Application and validation through the numerical simulation of the Z24 Bridge, Mech Syst Signal Process. 70–71 (2016) 578–600. https://doi.org/10.1016/j.ymssp.2015.08.027.

[77] Y. Wang, Z. He, Y. Zi, A demodulation method based on improved local mean decomposition and its application in rub-impact fault diagnosis, Meas Sci Technol. 20 (2009) 025704. https://doi.org/10.1088/0957-0233/20/2/025704.
[78] I. Provazník, J. Kozumplík, Wavelet transform in electrocardiography—data compression, Int J Med Inform. 45 (1997) 111–128. https://doi.org/10.1016/S1386-5056(97)00040-3.
[79] Marie Farge, Alex Grossmann, Yves Meyer, Thierry Paul, Jean-Claude Risset, Ginette Saracco, Bruno Torresani, Les ondelettes et le CIRM [Wavelets and CIRM], Gazette Des Mathématiciens. 131 (2012) 47–57. https://hal.archives-ouvertes.fr/hal-01136298.
[80] B. Adhikari, S. Dahal, M. Karki, R.K. Mishra, R.K. Dahal, S. Sasmal, V. Klausner, Application of wavelet for seismic wave analysis in Kathmandu Valley after the 2015 Gorkha earthquake, Nepal, Geoenvironmental Disasters. 7 (2020) 2. https://doi.org/10.1186/s40677-019-0134-8.
[81] A.T. Walden, A.C. Cristan, The phase–corrected undecimated discrete wavelet packet transform and its application to interpreting the timing of events, Proceedings of the Royal Society of London. Series A: Mathematical, Physical and Engineering Sciences. 454 (1998) 2243–2266. https://doi.org/10.1098/rspa.1998.0257.
[82] T. Kijewski-Correa, A. Kareem, Efficacy of Hilbert and Wavelet Transforms for Time-Frequency Analysis, J Eng Mech. 132 (2006) 1037–1049. https://doi.org/10.1061/(ASCE)0733-9399(2006)132:10(1037).
[83] M. Feldman, Hilbert Transform Applications in Mechanical Vibration, First Edit, John Wiley & Sons, Chichester, 2011.
[84] B. Boashash, Estimating and interpreting the instantaneous frequency of a signal. I. Fundamentals, Proceedings of the IEEE. 80 (1992) 520–538. https://doi.org/10.1109/5.135376.
[85] Paul C. Krause, Oleg Wasynczuk, Scott D. Sudhoff, Analysis of Electric Machinery and Drive Systems, Wiley-IEEE Press, 2002.
[86] H.M. Teager, S.M. Teager, Evidence for Nonlinear Sound Production Mechanisms in the Vocal Tract, in: Speech Production and Speech Modelling, Springer Netherlands, Dordrecht, 1990: pp. 241–261. https://doi.org/10.1007/978-94-009-2037-8_10.
[87] J.F. Kaiser, On a simple algorithm to calculate the “energy” of a signal, in: International Conference on Acoustics, Speech, and Signal Processing, IEEE, 1990: pp. 381–384. https://doi.org/10.1109/ICASSP.1990.115702.
[88] B. Boashash, Estimating and interpreting the instantaneous frequency of a signal. II. Algorithms and applications, Proceedings of the IEEE. 80 (1992) 540–568. https://doi.org/10.1109/5.135378.
[89] J.M. Londoño, S.A. Neild, J.E. Cooper, Identification of backbone curves of nonlinear systems from resonance decay responses, J Sound Vib. 348 (2015) 224–238. https://doi.org/10.1016/j.jsv.2015.03.015.
[90] N.E. Huang, Z. Wu, S.R. Long, K.C. Arnold, X. Chen, K. Blank, On Instantaneous Frequency, Adv Adapt Data Anal. 01 (2009) 177–229. https://doi.org/10.1142/S1793536909000096.
[91] A. Gelman, J.B. Carlin, H.S. Stern, D.B. Dunson, A. Vehtari, D.B. Rubin, Bayesian Data Analysis, 3rd ed., Chapman and Hall/CRC, New York, 2013. https://doi.org/10.1201/b16018.
[92] A.W. Bowman, A. Azzalini, Applied Smoothing Techniques for Data Analysis: The Kernel Approach with S-PLUS Illustrations, 1st ed., Oxford University Press, UK, 1997.
[93] M. Civera, C. Surace, A Comparative Analysis of Signal Decomposition Techniques for Structural Health Monitoring on an Experimental Benchmark, Sensors. 21 (2021) 1825. https://doi.org/10.3390/s21051825.
[94] Diana FEA BV™, DIANA FEA™ R10.5, (2021).
[95] Structural Vibration Solutions A/S, ARTeMIS Modal™ R6.1, (2020).
[96] The MathWorks Inc., MATLAB™ and Simulink™ Student Suite R2021a, (2021).
[97] The MathWorks Inc., MATLAB Wavelet Toolbox™ R2021a, (2021).
[98] M.G. Masciotta, D. Pellegrini, Tracking the variation of complex mode shapes for damage quantification and localization in structural systems, Mech Syst Signal Process. 169 (2022) 108731. https://doi.org/10.1016/j.ymssp.2021.108731.